THE ASTROPHYSICAL JOURNAL, 211:755–771, 1977 February 1

ON THE RELATIONSHIP OF INTERSTELLAR N_2H^+, HCO^+, HCN, AND CN

B. E. TURNER
National Radio Astronomy Observatory,* Green Bank, West Virginia
AND
P. THADDEUS
Goddard Institute for Space Studies
Received 1976 May 20; revised 1976 July 12

ABSTRACT

A survey of 73 sources has been made in the emission lines of N_2H^+ and HCO^+, including detailed maps of four sources (Ori A, OMC-2, DR 21 OH, and NGC 6334). These data are combined with equally extensive data for HCN and CN to make a detailed study of the spatial relationship of these four species. Actual abundance ratios are shown to vary, often sharply, over small scale lengths ($\sim 1'$) within our mapped sources. Excitation temperatures vary also. All four species appear to be subthermally excited. The abundance ratios, and their spatial variations, are interpreted in terms of ion-molecular formation and destruction processes. It is concluded that the relative abundances of CO may be considerably lower in some regions than previously believed. No evidence is found for variations in the C/O ratio over small scale lengths in Ori A. The degree of ionization of the Ori A molecular cloud may be significantly different from that of other molecular clouds.

Subject headings: interstellar: abundances — interstellar: molecules — molecular processes

I. INTRODUCTION

Mechanisms for the formation and destruction of interstellar molecules are not well understood. Considerable evidence favors ion-molecule reactions as a predominant process for *small* interstellar molecules (Herbst and Klemperer 1973, hereafter HK; Watson 1973, 1974), although such reactions seem unable to explain the presence of the larger interstellar species, which may well be formed on grain surfaces. Current knowledge of formation processes on grain surfaces is too imprecise to permit a decisive comparison with observations. However, ion-molecule reactions are considerably better understood and, despite uncertainties in some individual reactions, seem able to predict rather definitely the relative equilibrium abundances of a few of the simpler interstellar molecules.

Comparisons of these theories with observations are at present inconclusive because they rest on poorly determined abundances and on a small number of (perhaps) unrepresentative interstellar sources. A better comparison of theory and observations requires a judicious selection of molecular species and a detailed observational survey of the spatial relationship between those species. The chosen molecular species should have the following attributes: (*a*) they should constitute as critical a test of the theory to be examined as possible; and (*b*) they should be easily observable (with high spatial resolution) over a large number of interstellar regions. N_2H^+ (Turner 1974; Green, Montgomery, and Thaddeus 1974; Thaddeus and Turner 1975), HCO^+ (Woods *et al.* 1975; Snyder *et al.* 1976; Hollis *et al.* 1975), and HCN are among the few interstellar molecules that fulfill both criteria well. They have the added advantage of very similar excitation requirements. CN satisfies criterion (*b*) but satisfies criterion (*a*) less well. In this paper we describe the results of surveys of these four molecules, including detailed maps of them in the molecular clouds associated with Ori A, OMC-2, DR 21 OH, and NGC 6334. The data for N_2H^+ and HCO^+ were obtained by the present authors in 1974 September. The CN data are from Turner and Gammon (1975, hereafter TG). The HCN data are taken from Gilmore *et al.* (1977) and Morris *et al.* (1974), except for Ori A; those are from Snyder and Buhl (1977) and Gottlieb *et al.* (1975).

Rest frequencies for N_2H^+ and HCO^+ are discussed in § III, where our astronomically derived values are compared with recent laboratory determinations. Section IV presents the basic data. In § V, we discuss the correlation in the spatial distribution of these species, in a qualitative sense, and the factors (e.g., different opacities and possibly excitation) which limit the conclusions we may draw about the physical relationship. The correlations in spatial distributions are then examined quantitatively. In § VI, we try to separate the effects of opacity and excitation temperature by using the observed hyperfine (hf) ratios of N_2H^+, HCN, and CN. Reasons for the generally low excitation temperatures of these species are discussed. Having concluded that actual abundance ratios vary spatially, we discuss in § VII the chemistry of these species in terms of ion-molecule reactions. On this

* Operated by Associated Universities, Inc., under contract with the National Science Foundation.

basis, some conclusions are reached about atomic abundance ratios and their spatial variations, as well as the relative abundance of CO in the Ori A molecular cloud.

II. THE OBSERVATIONS

All observations were made with the NRAO 36 foot (11 m) telescope, equipped with an uncooled double-sideband mixer receiver whose single-sideband (SSB) system temperature was typically 1500 K. Spectra were obtained by switching the position of the telescope at 30 s intervals, and subtracting the OFF-source spectra from the ON-source spectra. For those sources for which extensive maps have been made, care was taken to ensure that the OFF-source position did not contain signals at levels of significance. No such precaution was taken for the unmapped sources in Table 1; for these a reference position 30′ away was typically used, except for L134 and Cloud 4, where preselected OFF positions were used.

The N_2H^+ and HCO^+ data were recorded on a spectrometer consisting of two banks of 256 filter channels, of widths 100 kHz and 250 kHz, respectively. Only 250 kHz data are available for the HCN data taken from Gilmore *et al.* (1977) and the CN data from TG.

All line intensities are in terms of brightness temperature, calibrated by means of a chopper wheel, and corrected for extinction by the Earth's atmosphere. These brightness temperatures assume that the source fills the antenna beam. The beam efficiencies and beamwidths of the 11 m telescope are as follows: 0.68 and 75″ for HCN and HCO^+, 0.67 and 71″ for N_2H^+, and 0.64 and 63″ for CN. Absolute pointing accuracy is estimated at 20″ (5 σ) and was monitored daily by pointing on Jupiter.

III. REST FREQUENCIES FOR N_2H^+ AND HCO^+

Accurate frequencies for these molecular ions have recently been measured in the laboratory. The rest frequency for HCO^+ is 89,188.545 ± 0.020 MHz (Woods *et al.* 1975). For N_2H^+, the measured frequencies are: $F = 1 \rightarrow 2$, 93,173.70 ± 0.04 MHz; $F = 1 \rightarrow 1$, 93,171.88 ± 0.04 MHz; $F = 1 \rightarrow 0$, 93,176.13 ± 0.18 MHz (Saykally *et al.* 1976). The velocities of astronomical sources radiating in these lines, as given in Table 1, are computed on the basis of these laboratory frequencies.

We have derived "astronomical" rest frequencies for HCO^+ and N_2H^+ by assuming that the radial velocities of these species in astronomical sources are the same as the velocity of HCN. Averaged over a total of 62 sources for N_2H^+ and 75 sources for HCO^+, we find astronomically determined frequencies of

$$\nu_0(N_2H^+) = 93{,}173.58 \pm 0.28 \text{ MHz},$$

$$\nu_0(HCO^+) = 89{,}188.55 \pm 0.27 \text{ MHz}.$$

Here, the uncertainties reflect directly the formal rms values for the average velocity differences $v(x) - v(\text{HCN})$, where $x \equiv N_2H^+$ or HCO^+. These uncertainties are considered to be conservative, because the broad-line sources (whose velocity determination is relatively poor) have been weighted equally with the narrow-line sources. Also, probable velocity differences between different species are included in these uncertainties. The N_2H^+ frequency refers to the $F = 2 \rightarrow 1$ component. Relative to this, the frequencies of the other hf components, determined astronomically, are given by Thaddeus and Turner (1975).

Our HCO^+ frequency is in excellent agreement with the laboratory value, and suggests that possible errors in the laboratory value, caused by ion drift velocities, are very small. Our N_2H^+ frequency compares well with the astronomical value of 93,173.67 MHz deduced by Thaddeus and Turner (1975) for the single source OMC-2. These astronomical values agree with the laboratory value for N_2H^+ within the uncertainties. However, we note that use of the laboratory frequency for N_2H^+ gives velocities which are consistently more positive than the velocities of the other molecular species (see Table 2). Use of the astronomically determined frequency would reduce (and in some cases remove) this possible discrepancy, by lowering the N_2H^+ velocities by 0.39 km s^{-1}.

IV. THE BASIC DATA

The basic quantity by which we compare the spatial distributions of N_2H^+, HCO^+, HCN, and CN is the integrated profile $\int T_B dv$. Table 1[1] gives this quantity (in units of kelvins km s^{-1}) as a function of position and source. The integrated profile is a sum over the hf components in the cases of N_2H^+, HCN, and CN. It includes the contribution from the "pedestal" when this exists, at several positions in Ori A and two positions in OMC-2. The radial velocities with respect to the local standard of rest (LSR) are also given in Table 1. They are determined by Gauss-fitting the line profiles (all hf components simultaneously where possible) of both 100 kHz and 250 kHz data, and taking a weighted average. The estimated uncertainty in the determined velocity is typically 0.3 km s^{-1} (5 σ) in these cases. For sources in which the hfs in N_2H^+ and HCN is severely blended, the 5 σ uncertainty is $\gtrsim$ 1.0 km s^{-1}. In Table 1 the observed rms for the velocity distribution over several sources is given; it typically exceeds the estimated uncertainties in determination. Thus actual velocity differences seem to exist over the mapped regions in Ori A, OMC-2, DR 21 OH, and NGC 6334. (A velocity gradient in Ori A near the Kleinmann-Low [KL] nebula is well known.)

Other parameters of the line radiation may be useful in comparing the distribution of N_2H^+, HCO^+, HCN, and CN. Brightness temperatures and line widths are given in Table 1. For N_2H^+ and HCN, with hfs, the data are presented as follows. If the intrinsic line width is significantly smaller than the hf splitting, then the

[1] Three dots in Table 1 indicate no observation, while a dash indicates an observation with no detection.

1977ApJ...211..755T

TABLE 1

OBSERVED LINE PARAMETERS

Source	Integrated Intensity (K km s^{-1})				T_B (K)				Velocity (km s^{-1})				Δv (km s^{-1})			
	N_2H^+	HCO^+	HCN	CN	N_2H^+	HCO^+	HCN	CN	N_2H^+	HCO^+	HCN	CN	N_2H^+	HCO^+	HCN	CN
Ori A (−1, 3)	3.80	...	15.8	29.1	1.43	...	3.90	1.42	+9.22	...	+9.29	+7.6	1.43	...	2.71	4.8
(−1, 2)	5.13	...	23.1	19.7	1.21	...	5.16	3.02	+9.04	...	+8.95	+9.5	2.16	...	2.71	2.9
(−1, 1)	4.24	...	28.1	36.1	1.43	...	6.21	4.08	+8.68	...	+8.65	+8.9	2.62	...	2.71	3.7
(−1, 0)	...	...	99.9*	35.0	...	...	10.3	4.15	...	...	+8.07	+7.6	...	...	3.25	3.7
(−1, −1)	...	...	50.1	47.5	...	...	8.2	4.63	...	...	+8.05	+7.6	...	...	3.32	4.5
(−1, −2)	...	...	54.4	27.9	...	...	8.1	2.11	...	...	+7.40	+9.5	...	...	3.65	5.8
(−1, −3)	...	...	37.5	34.1	...	...	6.0	1.94	...	...	+8.77	+8.4	...	...	3.38	7.7
(0, 6)	–	11.2	~2	...	–	4.51	~0.6	...	–	+8.72	?	...	–	2.77	?	...
(0, 5)	3.70	17.9	~4.5	13.6	1.27	6.79	~1.3	1.80	+10.20	+8.48	?	+9.7	1.43	2.78	?	3.7
(0, 4)	9.49	10.7	~14	29.1	1.81	5.12	~4.0	3.63	+10.29	+9.92	?	+9.7	2.63	2.23	?	3.2
(0, 3)	9.97	15.1	30.6	32.9	2.57	5.81	8.9	5.60	+10.25	+9.58	+9.42	+9.2	2.03	2.80	2.29	2.6
(0, 2)	6.76	27.1	33.6	40.6	1.89	8.17	8.6	5.25	+10.08	+9.44	+9.23	+10.0	2.51	3.20	2.42	3.4
(0, 1)	6.88	53.7	75.8*	49.3	1.31	10.09	10.0	6.98	+10.10	+9.26	+9.39	+9.5	3.95	4.37	3.67	3.2
(0, 0)	3.76	55.1	207.8*	45.2	0.94	12.27	17.2	4.97	+9.29	+8.66	+8.56	+8.4	3.27	4.11	3.85	4.8
(0, −1)	4.06	37.6	167.8*	52.2	1.21	10.32	13.4	6.06	+7.46	+7.93	+7.70	+7.6	2.98	4.10	3.9	5.0
(0, −2)	5.43	34.5	78.3	31.6	0.97	8.62	10.4	3.20	+7.18	+6.59	+7.53	+7.4	2.48	4.25	4.3	4.8
(0, −3)	...	...	40.8	56.4	...	...	7.7	3.34	...	...	+8.38	+9.2	...	...	3.1	7.4
(0, −4)	...	...	...	8.2	...	...	...	1.12	...	...	...	+9.5	...	...	...	3.2
(1, 5)	1.54	16.5	~8.0	26.9	0.77	5.96	?	6.55	+10.77	+8.60	?	+10.3	2.81	2.84	?	2.1
(1, 4)	12.5	29.0	~13.3	58.8	3.42	11.18	?	8.48	+10.34	+8.42	?	+9.5	2.39	2.67	?	2.8
(1, 3)	10.6	28.7	40.9	66.5	2.22	12.43	9.7	6.88	+10.18	+8.25	+9.65	+9.5	2.82	2.45	2.44	3.2
(1, 2)	9.01	25.4	37.1	32.9	2.64	11.03	9.5	6.69	+10.41	+8.44	+9.50	+9.5	2.26	2.30	2.17	2.6
(1, 1)	5.81	...	49.3*	39.2	1.09	...	13.8	5.23	+10.74	...	+9.75	+10.0	2.39	...	1.42	2.9
(2, 4)	3.92	22.4	~10.7	26.7	1.22	9.17	?	6.29	+ 9.70	+7.99	?	+10.3	1.80	2.75	?	2.4
(2, 3)	2.27	25.5	22.9	29.3	0.72	8.87	4.3	6.35	+10.34	+7.78	+8.88	+9.2	2.33	2.80	3.04	3.1
OMC-2 (−2, 0)	1.57	4.92	10.2	...	0.46	3.05	1.92	...	+12.52	+11.38	+10.14	...	3.40	1.55	2.81	...
(−1, 0)	8.04	11.6	20.5	...	2.36	5.15	4.97	...	+11.57	+11.32	+10.66	...	1.87	2.43	2.24	...
(0, 4)	...	8.80	13.5	...	...	5.07	4.32	...	...	+11.96	+10.79	...	...	1.63	2.24	...
(0, 3)	6.97	11.2	13.8	...	1.08	5.48	4.18	...	+12.16	+11.91	+11.18	...	3.02	1.92	1.99	...
(0, 2)	6.08	13.6	13.4	...	1.24	5.89	2.62	...	+12.15	+11.81	+11.07	...	1.73	2.22	2.05	...
(0, 1)	5.91	17.0	18.3	...	1.79	6.61	4.54	...	+12.16	+11.71	+11.29	...	2.34	1.99	2.62	...
(0, 0)	9.01	12.2	18.7	...	2.35	6.29	4.95	...	+11.75	+11.42	+10.90	...	2.14	1.93	2.03	...
(0, −1)	2.60	10.1	15.0	...	1.26	5.12	4.92	...	+11.41	+11.27	+10.52	...	1.74	1.98	2.29	...
(0, −2)	3.21	10.4	15.2	...	1.05	4.93	4.95	...	+11.16	+11.33	+10.16	...	1.92	2.27	2.44	...
(0, −4)	...	5.98	11.0	...	...	2.51	3.15†	...	...	+10.86	+9.80	...	...	2.24	2.42†	...
(1, 0)	3.64	8.82	20.0	...	1.30	5.80	7.51	...	+11.60	+11.34	+10.63	...	2.66	1.66	1.78	...
(2, 0)	0.51	7.29	11.6	...	?	3.78	3.91	...	?	+11.31	+10.25	...	?	1.53	1.90	...
NGC 2264 (−2, 0)	–	3.03	11.2	...	–	1.52	1.59	...	–	+7.47	+7.3	...	–	3.01	3.2	...
(0, 4)	–	7.11	...	...	–	1.96	...	...	–	+5.59	...	...	–	4.38	...	...
(0, 2)	1.09	9.75	13.8	...	0.76	3.80	2.22	...	+7.31	+7.76	+6.8	...	1.41	3.08	2.8	...
(0, 0)	10.5	25.1	27.3	9.49	2.16	3.85	3.29	1.18	+8.40	+8.36	+7.4	+7.5	2.88	5.78	3.8	3.2
(0, −2)	–	3.32	10.2	...	–	1.40	1.75	...	–	+7.11	+7.8	...	–	3.49	2.7	...
(2, 0)	–	7.96	8.02	...	–	1.82	1.02	...	–	+7.04	+9.2?	...	–	4.79	3.6	...
W51 (−1, 0)	...	34.7	...	16.9	...	2.25	...	2.46	...	+59.36	...	+59.7	...	17.42	...	3.7
(0, 1)	...	29.2	...	29.5	...	3.99	...	2.48	...	+58.12	...	+57.3	...	8.46	...	5.5
(0, 0)	15.4	42.0	74.8‡	58.9	1.40†	4.65	3.7‡	2.74	?	+57.45	+53.7‡	+56.4	13.07†	10.19	19.‡	12.7
(0, −1)	...	17.2	...	5.93	...	2.21	...	1.28	...	+57.03	...	+56.5	...	8.85	...	3.4
(1, 0)	...	32.2	...	8.54	...	2.96	...	1.60	...	+57.81	...	+57.1	...	12.41	...	2.1
NGC 6334 N (2, 4)	9.25	...	26.8	...	2.05	...	3.46	...	−3.17	...	−5.29	...	3.29	...	3.61	...
(0, 10)	9.25	...	10.5	...	?	...	?	...	?	...	−2.96?	...	?	...	?	...
(0, 8)	15.8	5.46	17.0	...	2.31	1.28	?	...	−1.11	−2.35	−4.56?	...	2.81	4.78	?	...
(0, 6)	32.2	17.3	14.0	...	2.93	2.73	1.97	...	−2.29	−2.36	−3.87	...	2.29	5.96	7.80	...
(0, 4)	60.2	16.8	33.7	...	4.83	3.45	2.05	...	−3.60	−4.11	−4.81	...	3.21	5.54	6.01	...
(0, 2)	55.7	28.5	49.1	...	3.78	3.81	3.83	...	−3.44	−4.16	−5.78	...	5.10	8.45	5.50	...
(0, 0)	30.9	32.2	62.7	30.1	2.17	4.31	5.89	1.62	−4.74	−5.91	−7.13	−6.6	4.59	8.22	6.53	6.1
(0, −2)	–	13.9	25.9	...	–	2.13	1.78	...	–	−3.49	−1.92	...	–	7.40	5.24	...
(0, −4)	–	8.01	13.5	...	–	1.83	?	...	–	−2.98	−3.11?	...	–	4.98	?	...
(−2, 4)	3.93	...	...	...	0.34†	...	...	...	−4.81	...	...	...	9.99†	...	...	...
(−2, −4)	–	10.2	27.4	...	–	2.51	4.34	...	–	−1.15	−1.99	...	–	4.44	4.64	...
(−4, −4)	5.42	14.0	45.2	...	1.14	3.68	8.35	...	−1.13	−0.61	−0.81	...	2.53	3.57	4.20	...
(−5, −6)	6.81	6.53	7.66	...	1.22	1.44	3.06	...	−1.17	−2.78	−3.39	...	2.39	5.00	5.56	...
(−5, −8)	4.07	6.13	...	...	1.17	1.96	...	...	+3.34	−0.81	...	...	1.98	2.78	...	...
(−6, −8)	12.5	20.3	38.6	...	1.85	4.91	7.48	...	+0.10	−1.26	−1.87	...	3.24	4.45	6.77	...

TABLE 1—*Continued*

Source	Integrated Intensity (K km s^{-1})				T_B (K)				Velocity (km s^{-1})				Δv (km s^{-1})			
	N_2H^+	HCO^+	HCN	CN	N_2H^+	HCO^+	HCN	CN	N_2H^+	HCO^+	HCN	CN	N_2H^+	HCO^+	HCN	CN
NGC 6334 N (−7, −6)	4.39	...	22.2	...	?	...	3.06	...	?	...	−3.03	...	?	...	5.56	...
(−7, −8)	2.92	17.7	38.6	...	?	4.90	6.12	...	?	−2.36	−2.92	...	?	4.22	4.34	...
(−9, −9)	0.42	9.08	18.9	...	?	1.86	4.54	...	?	−4.34	−3.95	...	?	5.42	4.61	...
NGC 6334 S (0, 0)	14.1	29.7	37.8	25.1	2.71	5.63	4.68	1.95	−5.66	−5.41	−4.82	−5.5	3.52	5.36	6.83	5.8
(0, 1.5)	0.88	4.34	~14.7	...	1.70	2.87	1.66	...	+2.43	−6.34	−8.39	...	1.99	4.29	2.50	...
NGC 7538 (0, 2)	1.25	–	...	...	?	–	...	...	?	–	...	...	?	–	...	...
(0, 0)	10.5	13.8	16.5	10.8	2.07	2.74	4.14	1.15	−57.11	−57.52	−57.7	−57.4	2.97	3.52	4.1	4.2
(0, −2)	1.96	1.87	..	...	?	?	...	...	?	?	...	...	?	?	...	...
(2, 0)	2.12	4.61	...	...	?	?	...	...	?	?	...	...	?	?	...	...
S	15.0	19.7	...	...	2.22	4.75	...	...	−55.9	−57.39	...	...	4.73	3.28	...	...
DR 21 OH (−2, −3)	0.24	7.72	13.0	...	–	1.70	2.69	...	?	−2.71	−2.6	...	?	2.71	2.2	...
(−2, −4)	2.82	3.92	24.7	...	0.38†	0.88	2.34	...	?	−0.71	−2.6	...	9.19†	5.51	4.2	...
(−1, 3)	1.67	7.92	16.9	...	0.75	2.05	2.14	...	−2.43	−3.31	−3.2	...	1.88	4.32	4.7	...
(−1, 2)	5.58	11.6	16.2	...	1.32	2.28	1.65/1.48	...	−2.88	−3.33	−2.3/−4.5	...	3.11	5.60	4.9	...
(−1, 1)	7.75	14.0	22.9	...	1.42	1.87	1.91/2.31	...	−1.86	−3.85	−2.4/−5.2	4.37	4.37	8.39	6.8	...
(−1, 0)	5.82	12.4	29.2	...	1.14	1.88	2.37/2.86	...	−2.26	−2.46	−1.4/−4.7	...	2.53	7.09	3.2	...
(−1, −1)	3.19	9.16	19.1	...	1.08	2.61	2.11/1.82	...	−2.60	−3.02	−2.2/−4.8	...	3.08	4.03	4.0	...
(−1, −2)	2.24	11.0	19.3	...	?	2.36	2.00	...	−2.77	−2.64	−3.0	...	?	49.20	3.8	...
(−1, −3)	0.20	15.4	37.6	...	0.24†	1.90	2.84	...	?	−4.21	−2.6	...	7.77†	?.42	5.3	...
(−1, −4)	2.68	10.5?	22.7	...	0.32†	?	2.75/2.48	...	+0.47	?	−1.5/−3.9	...	9.07†		4.0	...
(0, 5)	6.18	5.20	...	...	0.72	1.26	...	...	−2.93	−2.66	...	...	3.80	4.28	...	...
(0, 4)	6.96	9.16	13.5	...	1.86	2.23	1.35	...	−3.03	−4.03	−3.1	...	2.73	3.86	3.8	...
(0, 3)	14.2	12.2	22.2	...	3.00	3.35	2.40	...	−3.29	−4.03	−4.5	...	2.84	3.54	2.7	...
(0, 2)	17.2	12.1	22.4	...	2.81	2.81	2.65	...	−2.83	−4.14	−4.9	...	3.59	4.52	2.5	3.4
(0, 1)	18.2	21.3	22.5	...	2.35	2.89	2.69	...	−2.95	−3.12	−4.4	...	3.71	8.33	3.4	...
(0, 0)	21.2	17.6	32.6	22.5	3.24	3.66	2.98	2.28	−2.86	−4.17	−4.9	−5.5	3.69	4.94	2.5	...
(0, −1)	6.18	12.0	23.5	...	1.18	2.14	3.00	...	−3.06	−3.54	−4.5	...	3.46	5.94	3.4	...
(0, −2)	4.89	11.6	22.4	...	0.46†	1.89	1.74	...	−2.30	−2.39	−2.4	...	12.85†	6.90	5.9	6.1
(0, −3)	8.69	20.5	33.3	33.4	1.61	2.56	2.97/2.71	2.20	−1.68	−3.34	−2.9/−4.4	−2.1	3.11	9.44	5.2	...
(0, −4)	7.41	11.6	30.9	...	1.55	2.55	2.14/1.94	...	−1.42	−3.35	−1.6/−3.9	...	2.35	9.49	6.2	...
(1, 3)	6.40	...	7.65	...	1.48	...	1.31/1.22	...	−4.00	...	−2.2/−5.7	...	2.79	...	<7	...
(1, 0)	3.73	11.1	16.7	...	1.06	1.48	2.55	...	−2.74	−3.35	−2.2	...	2.05	8.01	2.5	...
BD 66°1675	...	...	...	–	...	...	...	–	...	...	...	–	...	...	...	–
W3	–	9.92	15.4	14.1	–	1.22	3.34‖	1.02	–	−38.8	−42.6	−39.4	–	9.71	6.8‖	7.7
W3 OH	7.96	14.1	...	11.4	1.48	2.5§	...	1.37	−45.8	−48.2	...	−48.6	3.61	5.0§	...	4.2
AFCLR-1	–	6.72	5.07	–	–	1.8§	0.75‖	–	–	−12.7	−14.1	–	–	3.5§	2.4‖	–
HD 21483	...	...	3.29?	2.28	...	...	?	1.0	...	...	?	+1.8	...	...	?	1.3
HD 46883	...	...	...	–	...	...	...	–	...	...	...	–	...	...	...	–
HD 154368	...	...	...	7.41	...	...	...	0.62	...	...	...	~8.7	...	...	...	5.8
HD 183143	...	...	...	–	...	...	...	–	...	...	...	–	...	...	...	–
AB Aur	...	...	–	–	...	...	–	–	...	...	...	–	...	...	...	–
NGC 1333	3.23	9.24	4.78	...	0.98	2.98	2.4#	...	+8.98	+8.00	+7.94	...	2.05	1.95	1.48#	...
NGC 1999	–	5.61	3.80	6.00	–	3.06	1.11‖	0.89	–	+9.23	+9.8	+9.9	–	2.27	3.3‖	2.9
NGC 2023	...	6.90	...	...	...	?	...	...	...	?	...	...	...	?	...	...
NGC 2068	–	–	...	...	–	–	...	...	–	–	...	...	–	–	...	...
C0206.9−16.0	1.30	5.74	8.88	5.18	0.76	3.26	1.71	0.89	+10.79	+10.38	+9.9	+9.8	1.11	1.93	1.9	3.7
Ori B	3.45	7.42	21.0	17.1	0.96	2.15	6.49‖	1.83	+11.39	+10.88	+11.0	+11.5	1.67	4.25	2.0‖	3.4
Rosette IR	–	–	...	–	–	–	...	–	–	–	...	–	–	–	...	–
IC 2162	2.14	5.95	15.1	12.6	0.62	1.91	2.07	1.37	+7.37	+7.86	+7.13	+5.8	2.97	3.38	2.94	5.5
S269	2.06	2.47	5.09	–	?	0.95	0.74	–	?	+16.78	+17.9	–	?	3.48	4.34	–
VY CMa	...	–	...	–	...	–	...	–	...	–	...	–	...	–	...	–
OH 0739−14	–	–§	–	–	–	–§	–	–	–	–§	–	–	–	–§	–	–
IRC 10216	–	–	71.0‡	18.1	–	–	3.5‡	0.60	–	–	−21.8‡	−25.1	–	–	~24‡	28.5
Y CVn	–	–	...	3.26	–	–	...	0.22	–	–	...	~3.4	–	–	...	14.3?
L134	–	–	...	...	–	–	...	...	–	–	...	...	–	–	...	...
L134 N	–	–	–	...	–	–	–	...	–	–	...	...	–	–	...	...
Cloud 4 (En)	1.37	2.61	...	...	0.46	0.56	...	...	+4.12	+2.87	...	...	2.05	1.26	...	...
Cloud 4 (NH_3)	–	...	–	–	–	...	–	–	–	...	–	–	–	...	–	–
H2-3	...	7.45	24.9‖	...	...	1.4§	2.72†‖	...	...	−19.7§	−21.4†‖	...	...	5.0§	13.2†‖	...
W22 A	...	...	14.0	...	...	...	1.55	...	...	...	−7.08	...	...	...	2.85	...
W22 B	...	9.66	9.05	...	...	1.4§	?	...	...	−3.7§	−2.60?	...	...	6.5§	?	...
Sgr A (NH_3 A)	42.7	45.3	...	–	1.56†	1.87	...	–	+26.9	+28.5	...	–	30.1†	28.7	.•.	–
Sgr A	...	–§	...	...	...	–§	...	...	...	–§	...	...	...	–§	...	...
Sgr A (NH_3 B)	–	...	...	...	–	...	...	...	–	...	...	...	–	...	...	...

TABLE 1—*Continued*

Source	Integrated Intensity (K km s^{-1})				T_B (K)				Velocity (km s^{-1})				Δv (km s^{-1})			
	N_2H^+	HCO^+	HCN	CN	N_2H^+	HCO^+	HCN	CN	N_2H^+	HCO^+	HCN	CN	N_2H^+	HCO^+	HCN	CN
Sgr B2 (0, 0)																
$v = 82$ }	30.9	129.	...	–	1.04†	1.32	...	–	+77.9	+84.9	+88.2**	–	17.8†	24.0?	...	–
$v = 50$ }					0.64†	1.10	...	–	+48.1	+72.6	+43.6**	–	32.0†	73.6?	...	–
Sgr B2 (0, 1)																
$v = 77$ }	26.7	108.	...	...	0.74†	2.55	...	...	+82.1	+92.1	...	...	20.1†	37.7?	...	...
$v = 48$ }					0.91†	1.13	...	...	+50.4	+46.6	...	...	21.1†	10.8?	...	...
Sgr B2 (0, −1)																
$v = 71$ }	34.4	76.4	...	...	1.26†	1.02	...	...	+71.7	+79.4	...	...	20.4†	16.1?	...	...
$v = 50$ }					1.15†	0.69	...	...	+50.3	+60.9	...	...	13.0*	34.1?	...	...
Cloud 12	–	...	...	–	–	...	...	–	–	...	...	–	–	...	...	–
G10.6−0.4	4.36	24.0	50.7	...	1.10	3.85	1.69	...	−1.98	−2.36	−3.66	...	3.48	6.30	3.48	...
W31 N	7.84	8.24	16.8	...	1.37	1.03	0.79	...	+14.6	+13.7	+7.1	...	4.36	9.17	4.59	...
W31 S	6.70	15.5	9.39	–	0.80	1.06	0.62	–	+13.8	+6.71	+1.62	–	6.38	11.71	5.02	–
M8	–	7.15	9.05††	1.74	–	2.1§	1.1††	1.6?	–	+9.8§	+10.4††	~7.7?	–	3.2§	5.0††	1.0?
R CrA	2.49	9.58	10.6	13.8	2.10	4.94	1.85‖	0.74	+6.80	+5.85	+6.3	+8.9	1.45	2.09	3.0‖	~5.3
M17 SW	27.7	18.4	118.	...	1.37	3.36	4.18#	...	+19.3	+19.5	+19.2	...	?	6.41	6.3#	...
W33 (cont.)	...	11.5	25.2	...	...	2.0	2.0			+35.6	+35.0			6.94	?	
W33 N	6.27	...	...	–	0.88	...	...	–	+37.3	...	...	–	8.05	...	...	–
W33 S (OH)	...	5.75§	...	...	...	1.2§	...	...	...	+35.8§	...	...	...	4.5§	...	...
W33 A	11.3	3.69	11.6	...	2.02	0.65	0.55†	...	+36.5	+36.4	+40.9†	...	5.60	4.73	28.5†	...
W33 B	5.03	–	3.31	...	0.86	–	0.65†	...	+30.5	–	+35.3†	...	4.19	–	5.54†	...
G19.6−0.2	–	...	7.81	...	–	...	0.58†	...	–	...	+38.3†	...	–	...	19.6†	...
G20.1−0.1	...	0.98?	–	...	...	?	–	...	...	?	–	...	...	?	–	...
G24.3+0.1	0.06?	...	–	...	?	...	–	...	~73?	...	–	...	?	...	–	...
UOA-19	–	4.68	8.54	–	–	1.1§	0.66‖	–	–	−5.2§	−5.0‖	–	–	4.0§	10.2‖	–
W41	–	...	...	...	–	...	...		–				–			
W43	–	–	4.15	–	–	–§	~0.5	–	–	–§	~94	–	–	–§	~12	–
W44 A	3.99?	...	...	...	~1.1?	...	...	...	~44?	...	...	...	~2?	...	...	...
W44 B	0.56?	...	...	...	~0.9?	...	...	...	~40?	...	...	...	~2?	...	...	...
W33 S (OH)	...	–	...	...	...	–§	...	...	...	–§	...	...	...	–§	...	...
W49 (1) $v = 3$ }	5.23	27.9	...	20.0	?	2.44	...	0.95	?	+2.04	...	+3.6	?	4.38	...	5.3
$v = 11$ }					?	2.28	...	0.78	?	+10.9	...	+10.8	?	8.62	...	6.1
G45.07+0.13	–	...	7.42	...	–	...	~1.0†	...	–	...	+59.0†	...	–	...	?	...
G45.1+0.12	–	...	5.57	...	–	...	~1.0†	...	–	...	+58.9†	...	–	...	?	...
G45.5+0.0	6.04	...	4.51	...	0.69†	...	~1.0†	...	+62.2	...	+59.7†	...	7.90†	...	?	...
G45.5+0.1	3.15	...	4.70	...	0.30†	...	~0.7†	...	+60.2	...	+56.6†	...	15.5†	...	?	...
K3-50	...	15.4	12.0	...	...	1.9§	1.43	...	...	−23.7§	−24.1	...	...	7.6§	7.82	...
K3-50 (OH)	–	...	5.39	–	–	...	0.75	–	–	...	−23.0	–	–	...	6.1	–
OH 69.5−1.0	7.92	12.8	7.53	...	1.46	1.49	0.54	...	+11.42	+13.3	+10.9	...	3.98	8.81	5.90	...
OH 77.9+0.2	–	...	...	...	–	...	...	...	–	...	...	...	–	...	...	...
W75 N	7.42	11.0	37.9	18.3	1.33	1.60	3.11‖	1.66	+9.78	+10.9	+10.7‖	+9.4	2.35	7.25	4.2‖	4.8
S146	–	...	...	...	–	...	...	...	–	...	...	...	–	...	...	...
DR 13	...	...	5.31	...	...	...	0.6	...	...	...	+4.42	...	...	...	~7.4	...
NML Cyg	...	–§	...	–	...	–§	...	–	...	–§	...	–	...	–§	...	–
Cas A	...	–§	...	–	...	–§	...	–	...	–§	...	–	...	–§	...	–

NOTE.—Positions (1950) are as follows: Ori A (0, 0) ($05^h32^m47^s.0$; −05°24′20″); OMC-2 (0, 0) ($05^h33^m00^s.0$; −05°12′34″); NGC 2264 (0, 0) ($06^h38^m28^s.0$; 09°32′06″); W51 (0, 0) ($19^h21^m27^s$; 14°24′30″); NGC 6334 N (0, 0) ($17^h17^m32^s.0$; −35°44′20″); NGC 6334 S (0, 0) ($17^h16^m06^s.0$; −35°55′00″); NGC 7538 (0, 0) ($23^h11^m36^s.8$; 61°11′48″); NGC 7538 S ($23^h11^m36^s.1$; 61°10′29″); DR 21 OH (0, 0) ($20^h37^m14^s.0$; 42°12′00″); BD 66°1675 ($23^h59^m39^s.5$; 67°08′12″); W3 ($02^h21^m55^s.0$; 61°51′54″); W3 OH ($02^h23^m17^s.0$; 61°39′00″); AFCRL-1 ($03^h23^m44^s.8$; 58°36′38″); HD 21483 ($03^h25^m42^s.0$; 31°12′12″); HD 46883 ($06^h33^m24^s$; 10°19′37″); HD 154368 ($17^h03^m08^s.4$; −35°23′05″); HD 183143 ($19^h25^m13^s$; 18°10′54″); AB Aur ($04^h52^m34^s.9$; 30°28′03″); NGC 1333 ($03^h25^m54^s.4$; 31°10′12″); NGC 1999 ($05^h34^m00^s.8$; −06°47′01″); NGC 2023 ($05^h39^m10^s$; −02°17′49″); NGC 2068 ($05^h44^m08^s.1$; 00°02′19″); CO 206.9−16.0 ($05^h39^m10^s.9$; −02°17′51″); Ori B ($05^h39^m13^s.5$; −01°55′57″); Rosette IR ($06^h13^m59^s$; 04°15′09″); IC 2162 ($06^h10^m00^s.0$; +18°00′00″); S269 ($06^h11^m46^s.5$; 13°50′35″); VY CMa ($07^h20^m55^s$; −25°40′11″); OH 0739−14 ($07^h39^m59^s$; −14°35′44″); IRC 10216 ($09^h45^m14^s.0$; 13°30′40″); Y CVn ($12^h42^m46^s.0$; 45°42′48″); L134 ($15^h50^m54^s$; −04°31′00″); L134 N ($15^h51^m28^s$; −02°45′30″); Cloud 4 (En) ($16^h23^m09^s.6$; −24°25′00″); Cloud 4 (NH_3) ($16^h24^m47^s$; −24°33′00″); H2-3 ($17^h06^m02^s$; −41°32′17″); W22 A ($17^h21^m29^s$; −34°06′00″); W22 B ($17^h22^m22^s$; −34°17′36″); Sgr A (NH_3 A) ($17^h42^m28^s$; −29°01′30″); Sgr A ($17^h42^m28^s$; −28°58′30″); Sgr A (NH_4 B) ($17^h45^m41^s$; −27°56′48″); Sgr B2 (0, 0) ($17^h44^m11^s$; −28°22′30″); Cloud 12 ($17^h44^m21^s$; −28°14′46″); G10.6−0.4 ($18^h07^m30^s.3$; −19°56′28″); W31 N ($18^h05^m58^s.4$; −20°05′26″); W31 S ($18^h06^m24^s.3$; −20°19′10″); M8 ($18^h00^m41^s.0$; −24°23′18″); R CrA ($18^h58^m27^s.8$; −37°01′27″); M17 SW ($18^h17^m26^s.5$; −16°14′54″); W33 (cont.) ($18^h11^m18^s.3$; −17°57′30″); W33 N ($18^h11^m47^s.0$; −17°54′00″); W33 S (OH) ($18^h11^m11^s$; −18°01′30″); W33 A ($18^h11^m44^s.6$; −17°52′57″); W33 B ($18^h10^m59^s.6$; −18°02′47″); G19.6−0.2 ($18^h24^m49^s.9$; −11°58′31″); G20.1−0.1 ($18^h25^m22^s.7$; −11°30′47″); G24.3+0.1 ($18^h32^m32^s.3$; −07°38′24″); UOA-19 ($20^h27^m34^s.5$; 40°01′50″); W41 ($18^h31^m27^s.4$; −08°58′18″); W43 ($18^h45^m00^s$; −02°00′00″); W44 A ($18^h53^m57^s.6$; 01°24′55″); W44 B ($18^h54^m06^s.4$; 01°22′26″); W44 S (OH) ($18^h54^m11^s$; 01°23′00″); W49 (1) ($19^h07^m49^s.0$; 09°01′18″); G45.07+0.13 ($19^h11^m00^s.4$; 10°45′44″); G45.1+0.12 ($19^h11^m07^s.0$; 10°46′42″); G45.5+0.0 ($19^h11^m46^s.1$; 11°07′06″); G45.5+0.1 ($19^h12^m04^s.4$; 11°04′15″); K3-50 ($19^h59^m49^s.9$; 33°24′18″); K3-50 (OH) ($19^h59^m59^s.4$; 33°26′01″); OH 69.5−1.0 ($20^h08^m09^s.8$; 31°22′41″); OH 77.9+0.2 ($20^h26^m42^s.3$; 38°57′14″); W75 N ($20^h36^m50^s.0$; 42°26′58″); S146 ($22^h47^m30^s$; 59°39′00″); DR 13 ($20^h29^m52^s.3$; 38°47′36″); NML Cyg ($20^h44^m39^s$; 39°55′42″); Cas A ($23^h21^m11^s$; 58°32′48″).

* Pedestal feature present; in these cases the total integrated intensity exceeds the sum of the integrated intensities of the three hf components.

† See text. ‡ Ulich and Haas 1976. § Hollis *et al.* 1975. ‖ Morris *et al.* 1974. # Gottlieb *et al.* 1975. ** Snyder and Buhl 1976 (private communication).

†† Giguere *et al.* 1973.

1977ApJ...211..755T

TABLE 2

CORRELATIONS BETWEEN INTEGRATED INTENSITIES

Region	Species	No. of Points	Average Velocity Difference	rms Velocity Difference	Correlation Coefficient ρ	Student's T-Test	Confidence Interval (%)	Least-Squares Fit Relation $y = (a \pm b) + (c \pm d)\cdot\chi^*$ a	b	c	d
Ori A.....	N_2H^+/HCO^+	15	+1.23	0.84	+0.036	0.132	88	+5.72	2.29	0.01	0.08
	N_2H^+/HCN	19	+0.50	0.75	−0.071	0.294	76	+5.93	1.02	0.00	0.01
	HCO^+/HCN	15	−0.44	0.74	+0.794	4.714	< 0.1	+18.6	2.88	0.18	0.04
	N_2H^+/CN	18	+0.47	0.51	+0.524	2.455	2.5	+1.66	1.90	0.12	0.05
	HCO^+/CN	14	−0.75	0.71	+0.526	2.142	5.0	+10.1	9.13	0.48	0.22
	HCN/CN	23	−0.08	0.66	+0.359	1.762	9.0	+32.8	0.30	0.09	0.01
OMC-2.....	N_2H^+/HCO^+	10	+0.33	0.35	+0.679	2.619	2.5	−1.47	2.48	0.58	0.22
	N_2H^+/HCN	10	+1.10	0.48	+0.620	2.235	5.0	−3.04	3.57	0.50	0.22
	HCO^+/HCN	10	+0.85	0.28	+0.522	1.731	12	3.04	4.54	0.49	0.28
NGC 6334.....	N_2H^+/HCO^+	16	+1.01	1.21	+0.563	2.551	2.2	−3.40	8.38	1.23	0.48
	N_2H^+/HCN	18	+1.61	1.23	+0.424	1.871	7.5	−0.12	8.80	0.52	0.28
	HCO^+/HCN	15	+0.55	0.95	+0.831	5.393	< 0.1	1.59	2.92	0.47	0.09
DR 21 OH.....	N_2H^+/HCO^+	21	+0.76	0.65	+0.577	3.083	0.6	−2.35	3.32	0.79	0.26
	N_2H^+/HCN	21	+0.88	0.79	+0.230	1.030	31	+2.89	4.21	0.18	0.18
	HCO^+/HCN	20	+0.20	0.85	+0.547	2.773	1.3	+4.36	2.92	0.34	0.12
Miscellaneous Regions.....	N_2H^+/HCO^+	45	+0.69	0.85	+0.784	8.281	≪0.1	+1.95	1.12	0.30	0.04
	N_2H^+/HCN	38	+1.28	1.18	+0.724	6.292	< 0.1	+0.83	0.79	0.17	0.03
	HCO^+/HCN	34	+0.67	1.06	+0.554	3.778	< 0.1	+5.37	1.58	0.19	0.05
	N_2H^+/CN	29	+0.71	1.40	+0.120	0.630	53	+4.61	2.17	0.10	0.15
	HCO^+/CN	31	+0.27	1.07	+0.176	0.960	35	+12.9	5.57	0.35	0.37
	HCN/CN	22	−0.06	1.32	+0.845	7.062	≪0.1	−0.08	0.27	0.54	0.01
All Regions.....	N_2H^+/HCO^+	107	...	...	+0.512	6.108	≪0.1	+3.06	1.18	0.29	0.05
	N_2H^+/HCN	106	...	...	+0.232	2.430	1.8	+4.80	1.18	0.07	0.03
	HCO^+/HCN	94	...	...	+0.714	9.792	≪0.1	+7.49	1.00	0.24	0.02
	N_2H^+/CN	51	...	...	+0.176	1.255	23	+5.03	1.76	0.08	0.07
	HCO^+/CN	49	...	...	+0.349	2.553	1.5	+12.6	4.24	0.41	0.16
	HCN/CN	49	...	...	+0.583	4.918	< 0.1	+14.4	0.19	0.27	0.01

* The b and d are 1 σ uncertainties. The first species listed is y and the second species is χ.

fitted brightness temperature and line width of the strongest (center) hf component is given in Table 1, without comment. If the intrinsic line width is too wide to allow resolution of the hf components, a single Gaussian is fitted and the results are given in Table 1 with a dagger. An upper limit for the brightness temperature in nearly all negative cases is 0.4 K.

Figure 1 presents integrated intensity maps of the Ori A molecular source in the lines of N_2H^+, HCO^+, HCN, and CN. These maps illustrate a number of aspects of the spatial relationships of these species discussed in § V. Figure 2 shows spectra of HCO^+ in Ori A. At positions (0, 0) and (0, 1), the pedestal feature, well known in HCN, may be seen clearly in HCO^+ also. At the other positions shown in Figure 2, an asymmetrical feature occurs on the low-velocity wing of the main feature.

V. THE RELATIVE DISTRIBUTIONS OF N_2H^+, HCO^+, HCN, AND CN

a) Qualitative Aspects

i) *Ori A*

N_2H^+, HCO^+, and CN peak strongly in brightness temperature (T_B) near the position (1, 4), while HCN shows no enhancement here. N_2H^+ and CN also show a peak in integrated intensity (W) at position (1, 4), while HCO^+ shows little pronouncement in W here, the line widths being narrower than at other positions. At the KL position (0, 0), HCO^+ and HCN show a maximum in both T_B and W. However, N_2H^+ shows a local *minimum* in both of these quantities at KL, while CN has a minimum in T_B but no clear minimum in W. For CN, the minimum in T_B at KL corresponds to a minimum in column abundance and a maximum in excitation temperature (T_s) (i.e., a maximum in total particle density; cf. TG). Because of poor sensitivity, we cannot establish a similar picture reliably for N_2H^+, but such a picture is consistent with our N_2H^+ observations. At position (1, 4) also, the CN results indicated a local peak in total particle density ($\sim 10^5$ cm^{-3}), although less than that generally attributed to KL, but no enhancement or reduction of CN column density.

Overall, N_2H^+ and CN appear to behave similarly, and quite differently from HCN, while HCO^+ seems to have some of the attributes of each category. This situation is not reflected in the line widths of these species. Averaged over the Ori A map, the line widths for N_2H^+, HCO^+, HCN, and CN are, respectively, 2.5, 3.1, 3.5, and 3.9 km s^{-1}.

The distribution of T_B for N_2H^+ falls off noticeably faster away from (1, 4) than that of either HCO^+ or CN. The distribution of W for these species is more similar in the vicinity of (1, 4).

The well-known velocity gradient along the north-south ridge centered on KL is clearly seen in the N_2H^+ and HCO^+ spectra. The gradient appears somewhat more pronounced in these species than in HCN and

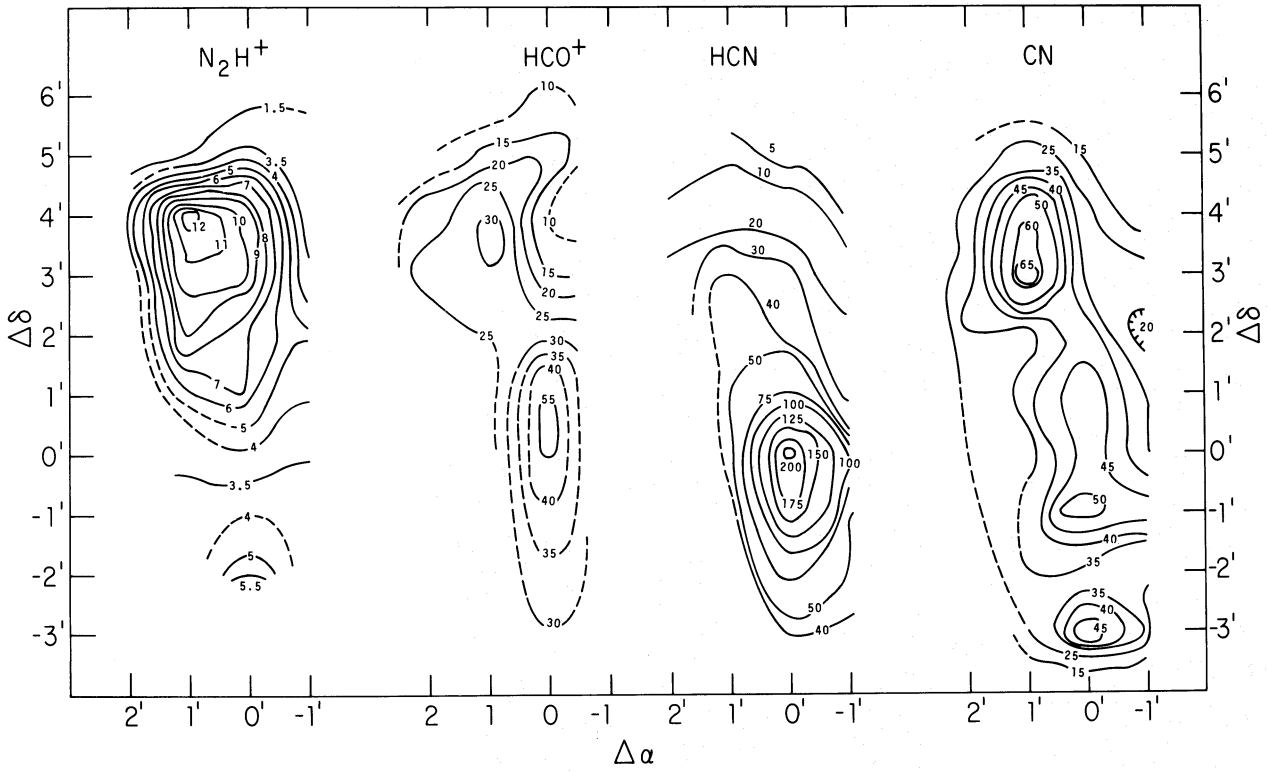

FIG. 1.—Contours of integrated intensity of N_2H^+, HCO^+, HCN, and CN for the Ori A molecular cloud. The (0, 0) position is that of the KL nebula. Contour units are kelvins km s^{-1}.

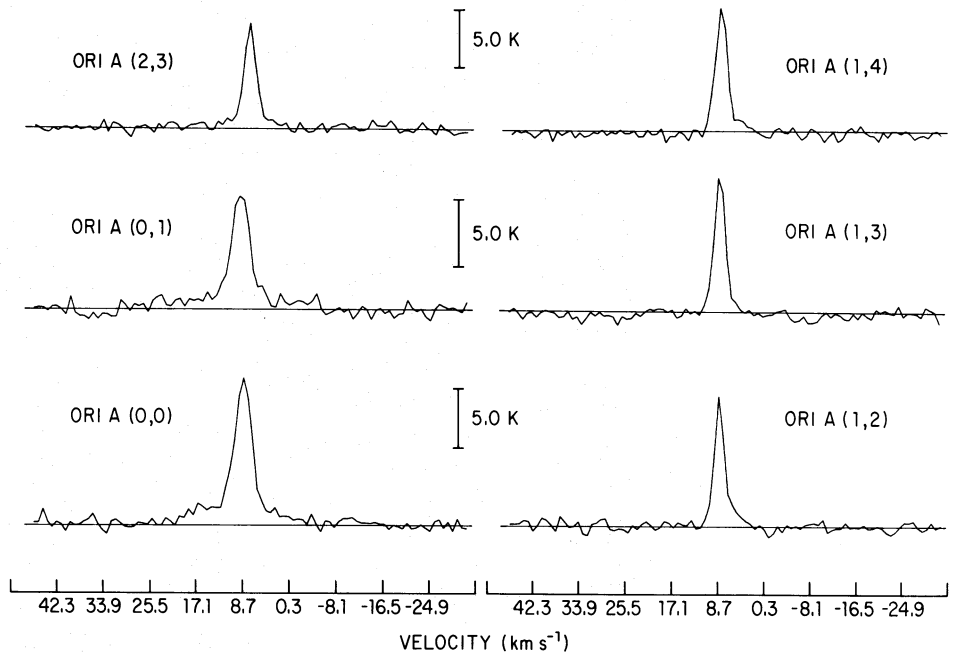

FIG. 2.—Selected spectra of HCO^+ in the Ori A molecular cloud. At positions (0, 0) and (0, 1), the "pedestal" feature may be seen clearly. At positions (1, 1), (1, 2), (1, 3), and (1, 4), the line is asymmetric and shows a weak broad feature on one side that resembles the "pedestal" at KL.

CN, but in all cases persists over a 5′ or 6′ range, from position (0, −2) to (0, 3) or (0, 4).

At KL, HCO^+ shows a wide-velocity component ("pedestal") similar to that of HCN (Gottlieb *et al.* 1975; Snyder and Buhl 1973), SiO (Dickinson *et al.* 1976), H_2S (Thaddeus *et al.* 1972), and SO (Gottlieb and Ball 1973). More important, this pedestal is present 1′ to the north of KL in the HCO^+ spectrum (Fig. 2). Either the pedestal source is centered ∼30″ north of KL, in which case it could be essentially a point source, or it is spatially extended, with a size of ∼1′. The pedestal source in HCN appears to be spatially extended (Snyder and Buhl 1977). The dominance of the spike over the pedestal is supposed to be a feature of organic molecules in the direction of KL (Zuckerman and Palmer 1975). Our spectrum of HCO^+ is consistent with this "rule," but it should be noted that the brightness of the HCO^+ pedestal actually exceeds that of the wide features of several inorganic species such as SiO, SO, and H_2S. If the HCO^+ pedestal is extended, then the usual argument, that the pedestal is weaker than the spike because it is severely beam-diluted, is precluded.

In the vicinity of the position (1, 4), our HCO^+ spectra show a distinct wing at the high-velocity side of the spike (Fig. 2). Except for its asymmetric nature, this feature has characteristics similar to the pedestal seen toward KL. It is clearly spatially extended.

The low-intensity, wide features seen in HCO^+ toward KL and position (1, 4) have no counterparts in our spectra of N_2H^+, although the latter is inorganic and therefore might be expected to exhibit a pedestal (Zuckerman and Palmer 1975). However, if the intensity ratio of pedestal to spike is the same for N_2H^+ and HCO^+, then we lack the sensitivity to detect an N_2H^+ pedestal.

ii) *OMC-2*

N_2H^+, HCO^+, and HCN all peak quite sharply in T_B near (0, 0), the position of the IR cluster (Gatley *et al.* 1974). However, the peaks appear to be displaced significantly, ∼30″ west for N_2H^+, ∼40″ north for HCO^+, and ∼40″ east for HCN. The integrated intensities W show the same behavior as T_B for N_2H^+ and HCO^+, while for HCN the integrated profiles show a broad peak centered at (0, 0). Brightnesses and equivalent widths fall off roughly monotonically away from (0, 0) for all three species. The falloff is fastest for N_2H^+ and least pronounced for HCN. The line widths are smaller than for any other region studied, being 2.3, 1.9, and 2.2 km s^{-1} for N_2H^+, HCO^+, and HCN, respectively, averaged over the map.

A pedestal feature occurs in the HCO^+ spectrum at position (0, 1), where T_B peaks (see Fig. 3). It is ∼15 km s^{-1} wide, or about half the width of the Ori A (KL) pedestal. The pedestal is not seen at adjacent positions in OMC-2. There is a possibility of a pedestal in HCN at (0, 0), of width ∼8 km s^{-1}. No broad-velocity features are seen in the N_2H^+.

iii) *DR 21 Region*

The distribution of T_B is very similar for N_2H^+, HCO^+, and HCN. All three species peak sharply at DR 21 OH (defined as position [0, 0]) and at DR 12 (3′ south of DR 21 OH), the value of T_B being somewhat higher at DR 21 OH, as is also true for CN.

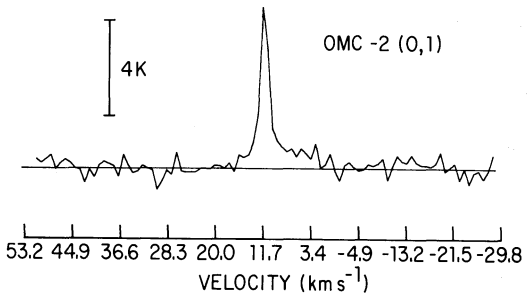

FIG. 3.—HCO^+ at position (0, 1) in OMC-2. A "pedestal" feature similar to that seen at KL in Ori A is apparent.

Analyses of both CN and N_2H^+ spectra (TG; Turner 1974) indicate higher T_s rather than enhanced opacities at DR 21 OH, so that the higher values of T_B at DR 21 OH indicate mainly higher particle densities. There is a slight enhancement in T_B for N_2H^+ and HCO^+ at position (0, 3).

The above comments hold also for the integrated intensities, except that, in the case of HCO^+, the maximum values of W occur at DR 21 and 1′ north of DR 21 OH. As with T_B, the distribution of W falls off much more steeply for N_2H^+ than for HCO^+ or HCN, as one moves away from DR 21 and DR 21 OH. The HCO^+ distributions fall off noticeably faster than those of HCN.

The line widths, averaged over the map, differ significantly. They are 3.1, 5.8, and 4.1 km s^{-1}, for N_2H^+, HCO^+, and HCN, respectively. No velocity differences occur which can be related in any obvious way with the line width differences. The differences in line widths might correspond to larger opacities in HCO^+ and HCN than in N_2H^+. However, we believe this to be true in most sources, particularly Ori A, where there are no similar differences in line widths.

iv) *NGC 6334*

The (0, 0) position of this map refers to the position of the northern OH maser source ($17^h17^m32^s$, $-35°44'20''$ [1950]), while NGC 6334 S refers to the southern OH maser ($17^h16^m36^s$, $-35°55'00''$ [1950]). At (0, 0), there is a distinct peak in both T_B and W for HCO^+ and HCN, but the same parameters exhibit a sharp minimum for N_2H^+. As in Ori A (KL), we may surmise that the abundance of N_2H^+ decreases in regions of increased density. Other enhancements in both T_B and W occur for both HCO^+ and HCN at positions (−4, −4) and (−6, −8). In these cases, surprisingly, N_2H^+ either shows no local effect (−4, −4), or actually has an enhanced T_B and W (−6, −8). Similarly, all three species show maxima in T_B and W at the position NGC 6334 S. Owing to partially unresolved hfs and partly to poor sensitivity, we cannot determine, for N_2H^+ and HCN, whether opacity or T_s increases at these "anomalous" positions. CN appears to have significantly higher opacity at NGC 6334 S than at (0, 0), but comparable T_s. The total density does not seem to exceed 2×10^4 cm^{-3} at either position (TG).

Averaged over the entire map, N_2H^+, HCO^+, and HCN have line widths of 3.1, 5.4, and 5.3 km s^{-1}, respectively. There seem to be significant differences in average velocity of all four species (see Tables 1 and 2); HCO^+ and HCN have similar velocities and line widths, while N_2H^+ seems to differ significantly in both velocity and line width from HCO^+ and HCN. Although velocity determinations are relatively uncertain for this source, owing to the large line widths, it appears that the larger scatter in velocities from position to position, and from species to species, is real.

Owing to the ragged distribution of mapping points for this region, we cannot say whether N_2H^+ falls off in intensity faster than HCO^+ or HCN, as one moves away from peak intensity positions.

v) *Other Sources*

Despite the large variation in expected physical conditions, the values of T_B of all species are always well below expected kinetic temperatures T_k. The value of T_B for N_2H^+ (summed over hf components) is comparable with that of HCO^+ in most sources, being significantly less in one or two cases (e.g., G206.9−16.0) and appreciably greater in only two cases (W31 N, W33 A). The scatter in ratio of T_B's for N_2H^+ to HCO^+ is, not surprisingly, larger than it is over any of the mapped regions described above. There is some tendency for line widths, and hence integrated intensities, of HCO^+ to exceed those of N_2H^+.

Some individual sources deserve comment.

W3.—The apparent "avoidance" of dense regions by N_2H^+ is illustrated well by the failure to detect N_2H^+ in W3 ($T_B \leq 0.25$ K). As shown by thermalized λ6 cm OH lines (Rickard, Zuckerman, and Palmer 1975), W3 appears to be one of the densest molecular regions known.

Cloud 4 (C II).—Our detection of N_2H^+ and HCO^+ are among the first observations of "high excitation" species in dark dust clouds (cf. Snyder and Hollis 1976 for a summary of similar detections in dark cloud L134). The radiative rates (Einstein A's) are higher for N_2H^+ and HCO^+ than for any other transitions so far detected in dark clouds.

Sagittarius B2.—Figure 4 shows spectra of N_2H^+ at the (0, 0) position. It is seen that the velocity structure is quite different for the two species. The HCO^+ emission that occurs above 100 km s^{-1} has no counterpart in N_2H^+ or HCN (CN is not detected toward Sgr B2). Only CO and H_2CO have high-velocity features that might correspond to HCO^+. At (0, 0), HCN has a major feature at 88.2 km s^{-1} (Snyder, personal communication) that appears to have a counterpart in both N_2H^+ and HCO^+. A lower-velocity HCN feature at 43.6 km s^{-1} has a corresponding N_2H^+ feature, but the HCO^+ counterpart at this velocity lies at position (0, 1), not (0, 0). At all three positions, N_2H^+ shows the two velocity features at ∼50 and ∼75 km s^{-1} that are typical of such species as CH_3OH, SiO, and others. However, the very broad distribution of HCO^+ in velocity at all three positions near Sgr B2 is qualitatively similar to the velocity distribution of CO rather than to any of the

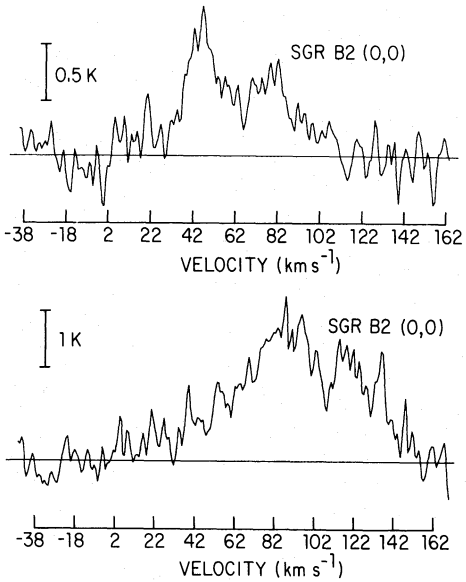

FIG. 4.—Spectra of N_2H^+ and HCO^+ at the (0, 0) position in Sgr B2. Note the different velocity ranges covered by the two species. The high-velocity (> 100 km s^{-1}) emission of HCO^+ is seen in CO and H_2CO, but in no other high-excitation species.

higher-excitation species. Of the sources we have studied, only in Sgr B2 does the velocity distribution of HCO^+ depart radically from that of the high-excitation molecules and instead emulate CO.

vi) *Summary of Qualitative Aspects of Relative Distributions*

1. It is common for N_2H^+ to be distributed differently from HCO^+ and HCN; the latter two species usually have quite similar distributions. N_2H^+ seems to avoid regions of high density, but HCO^+ and HCN do not. (In some regions, such as DR 21 OH, all three species have a similar distribution.) Where CN data exist, they indicate that CN and N_2H^+ are similarly distributed. (In Ori A, C_2H is distributed like N_2H^+ and CN, not like HCO^+ and HCN [Tucker and Kutner 1977].)

2. As mapped over extended molecular clouds, the values of T_B and W for N_2H^+ always seem to fall off away from peak areas faster than HCO^+ and HCN. HCN usually shows the slowest rate of falloff.

3. N_2H^+ line widths are nearly always smaller (often by a factor of nearly 2) than HCO^+ or HCN line widths. This is true for all of our mapped regions (when averaged over the maps) and for most of the miscellaneous sources. HCO^+ and HCN line widths are often quite different also; the wider widths belong to HCN in some sources and to HCO^+ in others. Sgr B2 is an extreme example of a wide HCO^+ profile.

4. Velocities for N_2H^+, HCO^+, HCN, and CN usually agree roughly within the uncertainties. However, a minority of sources (e.g., NGC 6334) may show significant velocity differences among the different species. Where velocity gradients are observed (e.g., Ori A, near KL), they are seen in all species.

5. In all sources, T_B (summed over hf components) is much less than the expected value of T_k.

6. T_B tends to vary relatively little for N_2H^+ from source to source. The variation is greater for HCO^+ and HCN. Thus, as averaged over all positions within a given mapped region, the ratio of (summed) T_B for N_2H^+ to that of HCO^+ has the value 1.47 for NGC 6334, 1.10 for DR 21 OH, 0.48 for OMC-2, and 0.35 for Ori A. The reason is that T_B for HCO^+ tends to be unusually high in OMC-2 and Ori A, rather than that T_B for N_2H^+ is unusually low. The brightness ratio averaged over all miscellaneous sources is 1.41.

b) Quantitative Aspects

We have derived the correlation coefficient ρ between integrated intensities (Table 1) for the different molecular species. For a given pair of species, ρ is defined as

$$\rho = \frac{m \sum x_i y_i - \sum x_i \sum y_i}{\{[m \sum x_i^2 - (\sum x_i)^2][m \sum y_i^2 - (\sum y_i)^2]\}^{1/2}},$$

where x_i and y_i are the integrated intensities of molecular species x and y, and m is the number of data pairs. We have also applied a Student's t-test to determine the level of statistical significance of the resulting correlation coefficients. Such a test is valid only if the variables involved have a normal distribution; such a distribution should characterize integrated intensities.

Table 2 presents correlation coefficients for the integrated intensities, source by source. In addition to the statistical information, we have listed the average velocity difference and its rms between the relevant pair of species as calculated for all data points for the source in question. The idea here is to see whether the degree of correlations may be related to kinematic circumstances rather than to reasons of abundance or excitation. No relation between the velocity difference or its rms and the correlation coefficient is apparent.

The correlation coefficients in Table 2 bear out the qualitative description given above. In the regions we have mapped (except for OMC-2), N_2H^+ shows little or no correlation with HCN, while HCO^+ is well correlated with HCN. N_2H^+ is uncorrelated with HCO^+ in Ori A, but is significantly correlated with HCO^+ in DR 21 OH and NGC 6334. In OMC-2, all pairs of molecules are roughly equally correlated. In Ori A, N_2H^+ and HCO^+ are about equally correlated with CN. This is because N_2H^+ correlates better with CN near the position (1, 4) while HCO^+ correlates better with CN near the position (0, 0).

This last example illustrates that the results of Table 2 can, through compactness, be misleading, and should not form the sole basis of subsequent analysis. The qualitative details of the distributions of each species in each mapped region are more important in understanding the physical and chemical relationship of these molecular species. It is clear that these relationships differ from region to region. For this reason, the correlation coefficients given for "miscellaneous" sources and "all sources" in Table 2 have limited meaning.

Table 2 also gives the parameters of a least-squares fit for an assumed linear relation of the form $y = (a \pm b) + (c \pm d) \cdot x$ between integrated intensities for pairs of molecular species. The results help further to point up differences in the distributions of the various species from source to source. For example, the slope of the HCO^+ versus HCN relation is significantly lower in Ori A than in the other mapped regions. Slopes of N_2H^+ versus HCO^+ and N_2H^+ versus HCN are also apparently lower in Ori A, although in these cases the pairs of variables are not apparently correlated in Ori A, while they are correlated in the other sources.

VI. DO THE RELATIVE ABUNDANCES OF N_2H^+, HCO^+, HCN, AND CN VARY SPATIALLY?

In order to explain the observations, we consider two possible molecular cloud models.

a) One has spatially constant relative abundances. This is equivalent to a "spatially invariant chemistry." In this model, the opacities for some species may be much greater than for others. Thus, for example, the brightness peak seen at Ori A (1, 4) in N_2H^+ and CN but not prominently in HCO^+ or HCN may imply only that the N_2H^+ and CN foreground opacities were small, while the HCO^+ and HCN foreground opacities were large. Or, the excitation of N_2H^+ and CN may somehow be enhanced relative to that of HCO^+ and HCN at Ori A (1, 4).

b) One has spatially varying relative abundances. In such a case, N_2H^+ (and CN) would have higher relative abundances at Ori A (1, 4) than elsewhere, and N_2H^+ would have lower relative abundance at the edges of the Ori A molecular cloud and at KL.

To distinguish between these models, we must try to separate the effects of opacity from those of excitation. This is difficult for HCO^+, because it has no hfs. The $H^{13}CO^+$ line has recently been detected (Snyder *et al.* 1976) at a frequency subsequently confirmed by laboratory measurements of Woods (1976, cited by Snyder *et al.* 1976). It is found that the integrated intensity ratio $T_B\Delta v$ (HCO^+)/$T_B\Delta v$ ($H^{13}CO^+$) varies from 8 to 22 for nine of the strongest sources of HCO^+, including Ori A, DR 21, DR 21 OH, W51, etc. In most sources the line width of $H^{13}CO^+$ is only about half that of HCO^+. These characteristics suggest that HCO^+ is optically thick in most sources, although possibly not in Ori A (KL), where the integrated intensity ratio is 22 (cf. Gottlieb *et al.* 1975).

a) *Hyperfine Ratios*

Estimates of opacity can be made for N_2H^+, HCN, and CN on the basis of their observed integrated hfs ratios. Table 3 presents this information for N_2H^+ and HCN. HCN data for positions $(0, x)$, $-2 \leq x \leq 3$ in Ori A are from Gottlieb *et al.* (1975); the remaining HCN data, of somewhat lower sensitivity, are from Snyder and Buhl (1977). HCN data for the other sources are taken from Gilmore *et al.* (1977). Similar data for CN have been given by TG.

For quantities involving hf components i and j, the integrated intensity ratio is computed as $T_{Bi}\Delta v_i/T_{Bj}\Delta_j$ and the formal 1 σ uncertainty as

$$\{[\sigma(T_{Bi})/T_{Bi}]^2 + [\sigma(T_{Bj})/T_{Bj}]^2 + [\sigma(\Delta v_i)/\Delta v_i]^2 + [\sigma(\Delta v_j)/\Delta v_j]^2\}^{1/2} .$$

All quantities in these expressions come from (simultaneous) Gaussian fits of the hf components. This formalism does not account for any correlation which may exist among the variables (e.g., the three hf line widths may be the same) or for any "nonlinear" errors which may occur in the fitting routine when the three hf components are blended (as in NGC 6334). These effects probably result in errors which are overestimated for Ori A and OMC-2, and underestimated for NGC 6334. For this reason, we will not discuss the NGC 6334 results further.

Opacities can be derived least ambiguously from hf ratios in the case of CN, for which all hf components except the strongest have approximately local thermodynamic equilibrium (LTE) brightness ratio. A direct interpretation of these ratios in terms of opacity, in which radiative trapping is neglected, seems justified. In this way TG find a modest peak in CN opacity at Ori A (1, 4) and a rather broad increase in T_s (i.e., total density) in the vicinity of (1, 4). At KL, on the other hand, the CN opacity is a minimum while the excitation is quite high. Unfortunately, CN has not been mapped in OMC-2, DR 21, or NGC 6334, although at a few observed positions its opacity is of order unity and its excitation is low ($\sim$6 K).

HCN is more complicated than CN because of clear anomalies in the observed hf components for some sources. In Ori A (Table 3) the relative intensity (R.I.) = 3 ($1 \rightarrow 1$) line is seen to be characteristically smaller relative to both the R.I. = 5 ($2 \rightarrow 1$) and R.I. = 1 ($0 \rightarrow 1$) lines than it would be in the optically thin case. Detailed calculations of Ori A HCN by Gottlieb *et al.* (1975) indicate that, of several possible excitation mechanisms, the one best able to explain the hf ratios and other observed characteristics involves collisions and a significant amount of radiation trapping in the λ1.7 mm transition connecting the $J = 2$ and $J = 1$ states. Resultant column densities ($\sim 10^{14}$ cm^{-2}) and opacities in the λ3 mm lines ($\gtrsim 1$) are modest, provided that the HCN is not clumped on a scale $< 1'$, and that the abundance ratio HCN/$H^{13}CN$ $\approx$ 25. However, an alternative case may be possible,[2] in which HCN/$H^{13}CN$ $\approx$ 90, the terrestrial carbon ratio. In this case the HCN column density and opacity are about 10 times higher. (In an earlier calculation, Kwan and Scoville [1975] favored an optically thick model for HCN also, although their calculation assumed no overlap of Doppler widths of hfs components.) The weight of evidence from these calculations, and from the fact that the line widths of HCN and $H^{13}CN$ are apparently the same, favors a $\tau \gtrsim 1$ model for Ori A HCN, although τ as high as $\sim$10 is also possible.

[2] Gottlieb *et al.* 1975 point out that this model may not correctly predict the observed hfs ratios of $H^{13}CN$, which have LTE values.

TABLE 3

INTEGRATED HYPERFINE INTENSITY RATIOS

Source	N_2H^+			HCN		
	$1 \rightarrow 1$ to $2 \rightarrow 1$	$0 \rightarrow 1$ to $1 \rightarrow 1$	$0 \rightarrow 1$ to $2 \rightarrow 1$	$1 \rightarrow 1$ to $2 \rightarrow 1$	$0 \rightarrow 1$ to $1 \rightarrow 1$	$0 \rightarrow 1$ to $2 \rightarrow 1$
Optically Thin	0.6	0.33	0.2	0.6	0.33	0.2
Ori A (−1, 2)	0.87 ± 0.33	0.31 ± 0.53	0.27 ± 0.50	0.40 ± 0.08	0.38 ± 0.08	0.15 ± 0.08
(−1, 1)	0.22 ± 0.47	0.75 ± 0.81	0.16 ± 0.67	0.39 ± 0.05	0.46 ± 0.05	0.18 ± 0.04
(0, 5)	0.88 ± 0.56	...	...	...	...	...
(0, 4)	0.51 ± 0.27	0.87 ± 0.42	0.44 ± 0.38	...	...	...
(0, 3)	0.78 ± 0.25	0.52 ± 0.35	0.41 ± 0.33	0.34 ± 0.02	0.53 ± 0.06	0.18 ± 0.02
(0, 2)	0.55 ± 0.28	0.31 ± 0.71	0.17 ± 0.68	0.37 ± 0.02	0.53 ± 0.06	0.19 ± 0.01
(0, 1)	0.49 ± 0.44	0.57 ± 0.76	0.28 ± 0.69	0.46 ± 0.03	0.67 ± 0.06	0.31 ± 0.03
(0, 0)	0.59 ± 0.56	...	...	* 0.48 ± 0.02	0.50 ± 0.06	0.24 ± 0.02
(0, −1)	0.51 ± 0.50	0.38 ± 0.98	0.19 ± 0.89	0.51 ± 0.03	0.48 ± 0.06	0.25 ± 0.02
(0, −2)	1.00 ± 0.45	...	...	0.48 ± 0.03	0.43 ± 0.06	0.21 ± 0.02
(1, 5)	0.34 ± 0.94	...	...	...	...	...
(1, 4)	0.70 ± 0.17	0.38 ± 0.47	0.26 ± 0.46	...	...	...
(1, 3)	0.40 ± 0.37	0.41 ± 0.91	0.16 ± 0.86	0.45 ± 0.03	0.38 ± 0.03	0.17 ± 0.03
(1, 2)	0.58 ± 0.15	0.35 ± 0.49	0.21 ± 0.48	0.45 ± 0.12	0.56 ± 0.12	0.25 ± 0.11
(1, 1)	0.89 ± 0.41	0.82 ± 0.54	0.73 ± 0.54	0.31 ± 0.11	0.58 ± 0.11	0.18 ± 0.11
(2, 4)	0.18 ± 0.53	0.75 ± 0.66	0.61 ± 0.60	...	...	...
(2, 3)	1.30 ± 0.62	...	...	0.43 ± 0.08	0.53 ± 0.08	0.23 ± 0.08
average	0.68	0.54	0.32	0.42	0.50	0.21
OMC-2 (−1, 0)	0.68 ± 0.30	...	...	0.77 ± 0.25	0.51 ± 0.45	0.39 ± 0.41
(0, 3)	0.91 ± 0.40	...	...	0.52 ± 0.44	0.23 ± 1.10	0.12 ± 1.03
(0, 2)	0.37 ± 0.76	...	...	0.35 ± 0.57	0.77 ± 0.93	0.27 ± 0.80
(0, 1)	0.66 ± 0.29	0.36 ± 0.69	0.24 ± 0.68	0.55 ± 0.23	0.25 ± 0.67	0.14 ± 0.65
(0, 0)	0.64 ± 0.10	0.40 ± 0.27	0.25 ± 0.26	0.55 ± 0.11	0.38 ± 0.23	0.21 ± 0.21
(0, −1)	1.03 ± 0.49	...	...	0.67 ± 0.36	...	...
(0, −2)	0.36 ± 0.25	...	...	0.36 ± 0.28	0.61 ± 0.48	0.22 ± 0.41
average	0.66	0.38	0.24	0.53	0.46	0.22
NGC 6334 (2, 4)	0.55 ± 0.34	0.62 ± 0.74	0.34 ± 0.71	0.77 ± 0.31	1.07 ± 0.34	0.83 ± 0.29
(0, 6)	...	...	0.45 ± 0.70	0.43 ± 0.73	0.60 ± 1.18	0.26 ± 1.16
(0, 4)	0.91 ± 0.40	0.36 ± 0.75	0.34 ± 0.70	0.61 ± 0.63	0.41 ± 0.64	0.25 ± 0.47
(0, 2)	0.45 ± 0.39	0.29 ± 0.98	0.13 ± 0.95	0.98 ± 0.47	1.15 ± 0.38	1.13 ± 0.51
(0, 0)	0.78 ± 0.49	0.46 ± 0.72	0.35 ± 0.69	0.80 ± 0.55	0.76 ± 0.39	0.61 ± 0.42
(−5, −8)	0.81 ± 0.75	...	...	0.13 ± 0.32	1.28 ± 0.44	0.17 ± 0.33
S(0, 0)	0.54 ± 0.29	...	...	0.29 ± 0.38	1.11 ± 0.43	0.32 ± 0.36
DR 21 OH (−1, 2)	0.51 ± 0.41	...	...	...	...	...
(−1, 1)	0.27 ± 0.45	0.92 ± 0.74	0.25 ± 0.64	...	...	...
(−1, 0)	0.99 ± 0.45	0.34 ± 0.70	0.34 ± 0.64	...	...	...
(−1, −1)	0.25 ± 0.75	...	...	...	...	...
(0, 4)	0.35 ± 0.43	0.77 ± 0.69	0.27 ± 0.58	...	...	...
(0, 3)	0.71 ± 0.18	0.51 ± 0.34	0.36 ± 0.32	...	...	...
(0, 2)	0.57 ± 0.19	0.61 ± 0.32	0.35 ± 0.30	...	...	...
(0, 1)	0.90 ± 0.29	0.55 ± 0.38	0.49 ± 0.36	...	...	...
(0, 0)	0.72 ± 0.27	0.47 ± 0.45	0.34 ± 0.42	...	...	...
(0, −1)	0.52 ± 0.52	0.31 ± 0.88	0.16 ± 0.82	...	...	...
(0, −3)	0.55 ± 0.33	...	...	...	...	...
(0, −4)	0.95 ± 0.36	0.61 ± 0.52	0.58 ± 0.49	...	...	...
(1, 3)	0.65 ± 0.37	0.37 ± 0.73	0.24 ± 0.69	...	...	...
average	0.61	0.55	0.34	...	...	...
NGC 2264 (0, 0)	0.54 ± 0.21	0.70 ± 0.35	0.38 ± 0.32	0.60 ± 0.05	0.43 ± 0.10	0.26 ± 0.03
NGC 7538 (0, 0)	0.97 ± 0.19	0.11 ± 0.54	0.12 ± 0.53	...	...	...
S	0.46 ± 0.19	0.36 ± 0.43	0.17 ± 0.41	...	...	...
W3 OH	0.51 ± 0.41	0.43 ± 0.68	0.22 ± 0.59	...	...	...
NGC 1333	0.91 ± 0.52	...	...	0.47 ± 0.07	0.56 ± 0.17	0.26 ± 0.06
G10.6−0.4	0.82 ± 0.47	0.58 ± 0.82	0.48 ± 0.79	...	...	...
W31 N	0.39 ± 0.30	...	...	...	...	...
W31 S	0.39 ± 0.63	1.14 ± 0.69	0.44 ± 0.53	0.94 ± 0.25	0.44 ± 0.36	0.41 ± 0.49
W33 N	0.13 ± 0.96	1.46 ± 1.21	0.20 ± 0.82	...	...	...
W33 A	0.25 ± 0.28	0.38 ± 0.56	0.10 ± 0.51	...	...	...
W33 B	0.48 ± 0.44	...	...	...	...	...
M17 SW	0.54 ± 0.43	0.60 ± 0.59	0.34 ± 0.54	0.46 ± 0.03	0.71 ± 0.03	0.34 ± 0.02
OH 69.5−1.0	0.61 ± 0.35	0.20 ± 1.06	0.12 ± 1.04	0.44 ± 0.86	1.17 ± 0.91	0.51 ± 1.08
W75 N	1.07 ± 0.44	0.60 ± 0.54	0.64 ± 0.52	...	...	...

* Gottlieb *et al.* 1975.

In OMC-2 (Table 3), the HCN hf ratios show similar, although weaker, anomalies. We may therefore expect HCN opacities to be smaller in OMC-2 than in Ori A.

No obvious hf anomalies occur for N_2H^+. Averaged over Ori A, Table 3 indicates that all three ratios are consistent merely with a small opacity (a few tenths). Despite the limited signal-to-noise ratio, there is a suggestion of an anomaly at position $(-1, 1)$, in the sense that the $1 \rightarrow 1$ line is unusually weak compared with the $2 \rightarrow 1$ and possibly the $0 \rightarrow 1$ lines. This is the same type of anomaly as is observed at *all* Ori A positions for HCN. The energy level configuration and spacing, and the dipole moment, are very similar for N_2H^+ and HCN. The rates for collisional excitation are also expected to be similar (Green 1975). Thus we may expect that the general presence of hf anomalies in HCN, and absence of them in N_2H^+, are due to appreciable optical depth in the HCN lines but not in the N_2H^+ lines.

In OMC-2, the N_2H^+ hf components have intensity ratios even closer to the LTE ratios than in Ori A. The three ratios given in Table 3 are all consistent with an N_2H^+ opacity of 0.1, and there is no indication of an anomaly at any position. Similar remarks apply to N_2H^+ in DR 21, except that the average opacity seems a little higher, as in Ori A.

In summary, the present evidence based on hf ratios and on isotope ratios suggests that HCO^+ and HCN are generally optically thick, while N_2H^+ and CN are generally optically thin. Qualitatively, this explains why the spatial distributions of intensity of HCO^+ and HCN are usually highly correlated but often differ significantly from the intensity distributions of N_2H^+ and CN, which themselves tend to be appreciably correlated. It remains to be seen whether HCN is optically thick enough to "obscure" possible locations of enhanced abundance, such as Ori A (1, 4). In sources like OMC-2, where all species appear to be optically thin, all are roughly similarly correlated in intensity.

b) Excitation Temperatures

Is the conclusion that HCO^+ and HCN are generally optically thick consistent with the fact (§ V*a*) that their values of T_B are comparable with the values of T_B for N_2H^+ and CN, which are concluded to be optically thin? Recall also that values of T_B for all four species are much smaller than estimated values of T_k taken from CO observations.

Under normal excitation conditions, large opacities cause T_B to approach the excitation temperature T_s in value, and T_s in turn to approximate T_k, for sufficiently large collision rates C. More specifically, T_s will approximate T_k for incoherent radiative scattering if the opacity exceeds the "thermalizing" value

$$\tau_{\rm th} = \frac{A + C[1 - \exp(-h\nu/kT_k)]}{C[1 - \exp(-h\nu/kT_k)]} .$$

This quantity is estimated at $T_k = 30$ K by using rate coefficients of $C \approx 10^{-10} n\ {\rm s}^{-1}$ for HCN (Green and Thaddeus 1974), $C \approx 5 \times 10^{-10} n\ {\rm s}^{-1}$ for N_2H^+ and HCO^+ (Green 1975), and $C = 10^{-10} n\ {\rm s}^{-1}$ for CN (TG). Then $\tau_{\rm th} \approx 1 + 6 \times 10^5/n$ for CN, N_2H^+, and HCO^+, and $\tau_{\rm th} \approx 1 + 2 \times 10^6/n$ for HCN. The total particle density n is very likely $\lesssim 5 \times 10^4\ {\rm cm}^{-3}$ in most of the sources considered here, so that opacities greater than 10 are needed to thermalize CN, N_2H^+, and HCO^+, and greater than 100 to thermalize HCN. Therefore the excitation temperatures of all species should be much less than the kinetic temperatures, as implied by the observations. Furthermore, although T_B should approach T_s more closely for HCN (and possibly for HCO^+) than for N_2H^+ and CN (because HCN and HCO^+ are optically thick), this effect might be compensated by a lower T_s for HCN, because it is farthest from being thermalized. Thus comparable brightness temperatures for all four species are not surprising. In only one case, the KL position in Ori A, might the density ($\sim 10^7\ {\rm cm}^{-3}$; Zuckerman and Palmer 1974) be high enough to thermalize all species.

The ratio R of integrated brightness of N_2H^+ to HCO^+ is ~ 1.4 averaged over NGC 6334 and over the miscellaneous sources. However, $R \approx 1.0$ averaged over DR 21, and ≈ 0.4 averaged over Ori A and over OMC-2. Specifically, the HCO^+ value of T_B is higher in Ori A and OMC-2 than in other regions, while T_B for N_2H^+ is more nearly the same over all sources. Because N_2H^+ and HCO^+ thermalize at very similar densities and have similar ratios of radiative to collision rates, any differences in T_s can arise only from different degrees of radiative trapping, i.e., from differences in abundances. Thus it is likely that the N_2H^+/HCO^+ abundance ratio is lower on the average in Ori A and OMC-2 than in the other cloud complexes.

Within OMC-2 itself, the brightness ratio R seems quite constant spatially. This seems to be because none of the species is particularly optically thick. In Ori A, the sharp changes in R at KL and at (1, 4) may occur for different reasons. At KL, we have the one case where the total density may be high enough to thermalize all four species (except possibly HCN). Then, since by observation $T_B < T_k$ for all species, they must all be optically thin (except possibly HCN). The spatial distribution of T_B for HCO^+ is a rather broad peak centered on KL. Since this peak is broader than that of the expected total density (Zuckerman and Palmer 1974), it is probable that T_s decreases, while τ increases, as one moves away from KL. That is, the HCO^+ abundance decreases somewhat near KL. For N_2H^+ and CN, the picture is much clearer, as there is an actual *minimum* in their brightnesses at KL. Since T_s cannot decrease at KL, the abundance of these species must decrease, and much more sharply than is the case for HCO^+. Near position (1, 4), R increases, but so does T_B for both N_2H^+ and HCO^+. Thus the HCO^+ cannot be very optically thick in this direction. According to TG, the CN abundance peaks at (1, 4) but the total density peaks to the south, at (1, 3) and (1, 2). The HCO^+ brightness also peaks at (1, 3), suggesting that an enhanced excitation is at least partly responsible. The N_2H^+ brightness, however, peaks at (1, 4) and may even have a shallow minimum at (1, 3).

Thus we again conclude that the abundance ratio N_2H^+/HCO^+ varies spatially near position (1, 4); N_2H^+ again is a more sensitive function of total density than HCO^+.

We summarize § VI as follows. HCN appears to be fairly optically thick in most sources ($1 \lesssim \tau \lesssim 10$), HCO^+ less thick, and N_2H^+ and CN generally optically thin. This explains why the brightness distribution of HCN is often poorly correlated with that of N_2H^+ and CN. All species are subthermally excited ($T_s \ll T_k$). The abundance ratio N_2H^+/HCO^+ seems to differ in different sources, and to vary over a given cloud complex (Ori A). The abundance of N_2H^+ (and CN) seems to depend more strongly on the total density than is the case for HCO^+. The abundance ratio N_2H^+/HCO^+ appears to drop sharply when the total density exceeds $\sim 10^5$ cm^{-3}.

VII. INTERSTELLAR CHEMISTRY OF N_2H^+, HCO^+, HCN, AND CN

Small molecules such as the four considered here are probably formed and destroyed in the interstellar medium primarily by gas-phase reactions including neutral and ion species. Previous analyses of observations of CN (TG), N_2H^+ (Turner 1974), and HCN (Gottlieb *et al.* 1975) have shown a general agreement with the predictions of the ion-molecule scheme of HK.

In Table 4 we list observed abundances of N_2H^+, CN (TG), and HCN (Gottlieb *et al.* 1975) in the few regions where these are considered most reliable. Total densities n are from TG and Gottlieb *et al.* The *relative* abundances of these species and HCO^+ are predicted to depend primarily on only two factors: total density, and the C/O abundance ratio. In what follows, we therefore stress the role of these aspects. We also indicate departures from the quantitative predictions of HK that may be expected because of revised reaction rates. The results are collected in Table 5, which is derived from HK and from Herbst *et al.* (1975).

In order to determine the likely causes of the discrepancies between observed and predicted ratios in Table 5, a summary of the reaction processes is in order.

N_2H^+ is formed 90% by direct reaction of H_3^+ and N_2, and 10% by reaction of N_2^+ and H_2, the N_2^+ coming from $He^+ + N_2$. Destruction is almost solely by reaction with CO and with CO_2, whose measured rate constants are almost identical. Hence the relative abundances of CO and CO_2 are not important in determining the abundance of N_2H^+. Herbst *et al.* (1975) have recently measured the rate constant for the dominant formation reaction $H_3^+ + N_2 \rightarrow N_2H^+ + H_2$ and find it to be only $\sim 2\%$ higher than the value estimated and used by HK. Also, Herbst *et al.* have calculated the N_2H^+ abundance for the cases C/O = 0.85 ("high" ratio) and 0.55 ("low" ratio) and find almost no dependence.[3] This is because of the assumption that essentially all C is tied up in CO or CO_2, the abundances of which do not therefore depend on C/O.

HCO^+ is formed predominantly by the reaction $H_3^+ + CO \rightarrow HCO^+ + H_2$. Much less important are the processes $C^+ + H_2O \rightarrow HCO^+ + H$ and $H^+ + CO_2 \rightarrow HCO^+ + O$. If the O/C ratio is high, then the reactions $C^+ + O_2 \rightarrow CO^+ + O$, $CO^+ + H_2 \rightarrow HCO^+ + H$ may become significant, because some of the excess oxygen is in the form of O_2. Unlike N_2H^+, HCO^+ cannot be destroyed by reaction with either CO or CO_2. The major destruction mechanism is $HCO^+ + e \rightarrow CO + H$, although a small fraction might be destroyed by $HCO^+ + H_2 \rightarrow H_3CO^+ + h\nu$. All reactions mentioned here for HCO^+ have measured rate constants except the last one involving radiative association. Because the presence of excess oxygen increases somewhat the net formation rate of HCO^+—but not the destruction rate—we expect the abundance of HCO^+ to be higher for the "low" C/O ratio. This is reflected in Table 5.

HCN is formed in the HK scheme primarily by $C^+ + NH_3 \rightarrow H_2CN^+ + H$ followed by $H_2CN^+ + e \rightarrow HCN + H$. Destruction of HCN is by reaction with C^+ and H_3^+. None of these reaction rates was measured at the time of the HK study. Recent measurements by Schiff *et al.* (1974) suggest a revision of this picture. They claim the formation reaction $C^+ + NH_3$ produces 95% NH_3^+ and only 5% H_2CN^+, although the net reaction rate constant is within 10% of the value used by HK. Also, the formation reaction $H_2CN^+ + e$ is said to produce more HNC than HCN (HNC will not isomerize to HCN at low temperatures). Subsequent measurements by Huntress (private communication) call into question the results of Schiff *et al.* and suggest instead that the formation reaction rates for HCN are close to those

[3] The C/H ratio is the same for both cases (3.75×10^{-4}); the O/H ratio differs.

TABLE 4

OBSERVED ABUNDANCES

Source	log n	log [HCN]	log [CN]*	log [N_2H^+]*
Ori A (0, 0) (KL).....	5.5	14.3†	14.2	< 13.0
Ori A (0, 2).....	5.0	14.3†	14.2	≲13.0
Ori A (−1, 2).....	4.5	...	14.0	13.2
M17 SW.....	4.5	14.3†	...	13.2
Ori A (0, 5).....	4.0	...	14.4	13.3
OMC-2 (0, 0).....	< 4.0?	13.2*	...	12.7

* Assumes no trapping effects.

† Gottlieb *et al.* 1975.

TABLE 5

PREDICTED ABUNDANCE RATIOS BY ION-MOLECULE REACTIONS

RATIO	C/O‡	PREDICTED* $n = 1 \times 10^4$	3×10^4	1×10^5	3×10^5	1×10^6	OBSERVED†
N_2H^+/HCN.....	0.85	0.013	0.011	0.007	0.008	0.008	$\lesssim 0.1$
	0.55	0.05	0.087	0.33	0.70	...	
N_2H^+/CN.....	0.85	0.002	0.002	0.002	0.003	0.002	$\lesssim 0.1$
	0.55	0.025	0.07	0.25	0.70	...	
CN/HCN.....	0.85	8.3	7.1	4.0	3.0	4.0	~ 1
	0.55	2.0	1.25	1.33	1.0	0.1	
N_2H^+/HCO^+.....	0.85	0.008	0.004	0.002	0.001	0.001	< 1
	0.55	0.003	0.001	0.001	0.0004	...	
HCO^+/HCN.....	0.85	1.66	2.86	4.00	7.00	6.00	$\lesssim 1$?
	0.55	20.	75.	300.	2000.	1000.	

* HK (1973); Herbst *et al.* (1975).

† Independent of density for $10^4 \leq n \leq 3 \times 10^5$ cm^{-3}, within the uncertainties.

‡ O/H is varied while C/H is held constant at 3.75×10^{-4}.

used originally by HK. In view of these contradictions, we adopt the original estimates of [HCN] by HK for use in Table 5. HK find that [HCN] depends strongly and directly on the value of C/O. If the Schiff *et al.* results are found to be correct, the effect will be to reduce [HCN] by a factor of ~ 40. The reduction factor will not depend on C/O to first order.

CN is thought to be formed by the exchange reactions N + CH and C + NH, and by the recombination reaction $H_2CN^+ + e$. It is probably destroyed by reaction with O, N, H_3^+, and He^+ as well as by adsorption on grains. The latter is possibly significant, because all of the gas-phase destructive reactions appear to be very slow at low temperatures. None of the reactions involving CN has been measured, so the predicted abundance of CN is very uncertain.

In addition to the abundance ratios given in Table 5, these reaction schemes (cf. HK) predict the following behavior:

1. $[N_2H^+]$ should be independent of n for $n \gtrsim 10^4$ (because H_3^+ and CO/N_2 are independent of C/O for $n \gtrsim 10^4$).
2. $[N_2H^+]$ should be independent of C/O for $n \gtrsim 10^4$ (because [CO] and $[N_2]$ are independent of C/O for $n \gtrsim 10^4$).
3. [CN] should be independent of n for $10^4 \leq n \leq 10^6$.

Table 5 indicates some severe discrepancies between observed and predicted abundance ratios, especially for the HCO^+/HCN ratio. For the case C/O = 0.85, the observed and predicted ratios can be brought into better agreement if the predicted abundance of HCN is increased by $\gtrsim 10$ times, and the abundance of N_2H^+ by a similar factor. (The abundance of CN appears to be consistent with observations, as found by TG.) For the case C/O = 0.55, the predicted abundance of HCN must be increased even further, and the abundance of N_2H^+ perhaps somewhat less, in order to get agreement.

Discrepancy between prediction and observations also occurs for the behavior of $[N_2H^+]$ as a function of n. Observationally, $[N_2H^+]$ (§§ V, VI) and CN (TG) both appear to decrease markedly for $n \gtrsim 10^5$, contrary to prediction. HCO^+ seems observationally to show a similar, but less pronounced, decrease with increasing n, a behavior again not predicted.

Most of these discrepancies can be removed by reexamining only one assumption made by HK, that of the abundance of CO. HK assumed $C/H = 3.75 \times 10^{-4}$ and calculate that virtually all C is tied up in CO. We consider two cases.

Case A.—Suppose that $C/H = 3.75 \times 10^{-4}$ is correct, but that only a small fraction (say 10%) of C is in CO. CO would therefore be 10 times less abundant than obtained by HK (independent evidence for this exists in studies of the excitation of CO by Leung and Liszt 1976). Also, C^+ would most likely be more abundant than assumed by HK, because several important reaction chains convert C^+ into CO (see, e.g., Glassgold and Langer 1976), so that less CO implies a reduced efficiency of this conversion. Then the following consequences would (qualitatively) occur:

1. The abundance of N_2H^+ would increase by a factor of over 10, because the primary destruction rate due to CO would be correspondingly reduced, and the abundance of H_3^+ increased.
2. Electron recombination, $N_2H^+ + e \rightarrow N_2 + H$, might start to compete with CO as a destruction mechanism for N_2H^+. As n increases, $[e]$ decreases more slowly than [CO] increases (cf. HK), so the net destruction rate would increase, and $[N_2H^+]$ would decrease with increasing n, as observed.
3. The abundance of HCO^+ will be reduced, although only by a small factor.
4. The abundance of CN will not change much from that predicted by HK.
5. The abundance of HCN should increase, because of more C^+. This is not evident from the foregoing, where C^+ was involved in both the principal formation and destruction reactions. However, when $[C^+]$ is appreciable, another formation sequence for HCN (Dalgarno and Oppenheimer 1974) can become significant: $C^+ + H_2 \rightarrow \cdots \rightarrow CH_3^+$ followed by $CH_3^+ + N \rightarrow H_2CN^+$ and $H_2CN^+ + e \rightarrow HCN + H$. Since

C^+ is involved in both formation mechanisms in the same way, the ratio of net formation rate to destruction, and hence [HCN], probably cannot be increased by more than a factor of 2 in this way. (It should be noted that [HCN] is dependent upon O/H and C/H as well as C/O.)

6. The increased available C^+ would enhance the buildup of larger carbon chain molecules such as CH_3CN and HC_2CN. It seems doubtful that observed quantities of these species could be produced by ion-molecule processes, unless $[C^+]$ is appreciable.

Case B.—If, on the other hand, C/H is (say) 10 times less than assumed by HK, but nearly all C is tied up in CO, then both CO and C^+ have reduced abundances. Statements (1) and (2) on N_2H^+ still apply. $[HCO^+]$ is slightly reduced (by a factor somewhat larger than in case A) because it is formed from CO and C^+ but not destroyed by either. The abundance of HCN will be roughly unchanged from Table 5, but the abundance of CN will be reduced because it is formed from C or CH.

We draw the following conclusions from this discussion.

1. Either a depletion of C, or a decrease in the fraction of C tied up in CO, will tend to produce better agreement between observations and theory for those ratios in Table 5 not including HCN. Better agreement with the observed dependence of $[N_2H^+]$ on n is also achieved.

2. With large uncertainty, we may prefer the case with no overall depletion of C, but only a small fraction of C in CO. This is because the predicted abundance of CN in this case seems best able to describe the observations, although the reaction rates involved in the CN equilibrium are very uncertain. Also, observed abundances of CH_3CH and HC_2CN seem to require appreciable amounts of C^+, if they are formed by ion-molecule reactions.

3. The underabundance of predicted [HCN] remains a possible problem, although within the observed uncertainties there may be no discrepancy.

Oxygen and Carbon Abundances:—When $[N_2H^+]$ is increased by a factor $\gtrsim 10$ and $[HCO^+]$ is decreased slightly in Table 5, improved agreement between predicted and observed ratios is achieved, for the high C/O ratio. The lower C/O ratio seems definitely less preferred, because it predicts too large a value for N_2H^+/HCN and HCO^+/HCN.

Note that the observed ratios in Tables 4 and 5 apply essentially only to the Ori A and OMC-2 regions. Zuckerman and Palmer (1975) have argued that the KL nebula in Ori A contains a lower C/O ratio than does the rest of the Orion molecular cloud. This does not apparently mean that C/H (i.e., CO) is lower at KL, because we observe a decrease, not an increase, in $[N_2H^+]$ at KL. Also, abundances of carbon molecules such as CH_3CN and HC_2CN peak close to or at KL. Therefore O/H must peak at KL. This should have no effect on $[N_2H^+]$ and should produce a minimum in [CN], as observed. However, according to HK, it should also increase $[HCO^+]$ and very sharply decrease [HCN] at KL, both of which contradict observations. On the basis of ion-molecule formation schemes, we conclude therefore that C/O is probably not different at KL. (The dominance of inorganic oxygen-bearing species such as SO, SO_2, and SiO at KL may well reflect a requirement of higher temperatures, such as exist at KL, for their formation.)

In § VI we indicated that $[N_2H^+]/[HCO^+]$ appears to be lower in Ori A and OMC-2 than in other regions. Is $[N_2H^+]$ lower, or is $[HCO^+]$ higher? Analyses of CN (TG) and HCN (Gottlieb *et al.* 1975) are consistent in showing that the excitation temperatures of these species, rather than their abundances, are higher in Ori A than in other sources. Therefore Ori A appears to be more dense on average, and the excitation temperatures of N_2H^+ and HCO^+ should also generally be higher. However, since T_B for N_2H^+ is not higher in Ori A, its opacity is implied to be smaller than in other sources, although there is no evidence for this conclusion from the observed hf ratios (Table 3). Because the uncertainties in observed hf ratios are high, and because they may not accurately reflect opacities directly, we regard the most likely picture as one where the abundances of CN, HCN, and HCO^+ do not differ greatly between Ori A and other sources, while N_2H^+ is of lower abundance in Ori A. There are two possible reasons. (1) The ratio N_2/CO is lower in Ori A; this would probably mean N/C is lower. (2) The degree of ionization is higher in Ori A (and electron recombination is competitive with reaction with CO in destroying N_2H^+).

In case $[N_2H^+]$ is similar in Ori A and other sources, while $[HCO^+]$ is higher in Ori A, the simplest explanation would be a *lower* degree of ionization in the Ori A cloud (since electron recombination is the only certain way of destroying HCO^+). If $[e] \approx [C^+]$, then variations in $[e]$ affect [HCN] and [CN] relatively little, but have a large and opposite effect on $[N_2H^+]$ and $[HCO^+]$.

VIII. CONCLUSIONS

Reasonably detailed maps of several extended molecular clouds in the emission lines of N_2H^+, HCO^+, HCN, and CN have indicated several rather general characteristics about the relative spatial distributions, and other properties. Among these are: (i) brightnesses of HCN and HCO^+ often correlate well, on the one hand, and brightnesses of CN and N_2H^+ correlate well, on the other. Rarely do N_2H^+ and HCO^+, or N_2H^+ and HCN, correlate well. (ii) N_2H^+ and CN are probably optically thin in most sources, HCN is usually quite thick, and HCO^+ is probably intermediate. (iii) The abundance ratio N_2H^+/HCO^+ appears to differ for different cloud complexes, and to vary spatially over a given cloud complex. (iv) The abundances of CN and N_2H^+ seem to depend more strongly on total density than do HCO^+ or HCN; [CN] and $[N_2H^+]$ decrease with increasing total density n, when $n \gtrsim 10^5$ cm^{-3}.

Best agreement is obtained between theory and observation when the abundance of CO is lower (by perhaps a factor of 10) than the value used by HK.

This suggests that either C in general is depleted, or that the fraction of C tied up in CO is small. No evidence is found for a different C/O ratio at the KL nebula in Ori A than applies to the rest of the Ori A cloud. A rather different degree of ionization is implied for the Ori A (and OMC-2) clouds than for other sources, based on a significantly different N_2H^+/HCO^+ abundance ratio in Ori A (and OMC-2).

It is unfortunate that firm quantitative conclusions about the details of (ion-molecule and other gas-phase) interstellar chemistry are difficult to draw even from fairly detailed observations of what we consider to be perhaps the four most basic "test" species. Generally speaking, the ion-molecule chemistry continues to describe, qualitatively and even semiquantitatively, the relative abundances and other properties of the spatial distributions as deduced from observations. However, a quantitative and rigorous test of the ion-molecule picture is still lacking. An equally desirable ultimate goal is a sufficiently detailed interpretation of the observations in terms of this picture to allow other astrophysical aspects to be understood, such as atomic abundance ratios (particularly the state of depletion of carbon and some other elements), the state (and cause) of ionization, the role of grains (as sources or sinks of interstellar molecules), and so on.

The failure to achieve such goals stems, unfortunately, from lack of precise information on a variety of fronts. Observationally, we require more extensive, and higher-quality, observations of CN, HCN, and N_2H^+ to determine, in many more types of sources and with much greater precision, how their hf ratios behave. For all four species, but particularly for HCO^+, information on isotopic species is essential. Detailed calculations, like those of Gottlieb *et al.* (1975), must be applied to CN and N_2H^+, as well as to HCN, and over a variety of sources.

Measured reaction rates for a variety of processes, especially those involving CN and HCO^+, are needed. *None* of the basic reactions governing CN has been measured. Electron recombination is the only certain destruction path for HCO^+. Whether HCO^+ is destroyed by reaction with H_2 is uncertain. And although HCO^+ is an extremely stable species, many other possible destruction pathways considered and rejected by HK are estimated to be only *slightly* endothermic. If some of them are actually slightly exothermic, they will become dominant destruction pathways. The present controversial measurement of the reaction of C^+ and NH_3, which probably dominates the interstellar HCN equilibrium, perhaps indicates the degree of difficulty to be expected in resolving some of these laboratory problems. It may be necessary to determine even the temperature dependence of all relevant reactions accurately. For example, the appearance of a "pedestal" velocity feature in HCO^+ but not N_2H^+ at the KL nebula in Ori A may well be explained in terms of the higher temperature thought to occur in this region, rather than by any difference in atomic abundance ratios there.

We thank W. Gilmore, M. Morris, P. Palmer, B. Zuckerman, D. Buhl, and L. E. Snyder for permission to use unpublished HCN data. We appreciate informative discussions on aspects of interstellar chemistry with E. Herbst.

REFERENCES

Dalgarno, A., and Oppenheimer, M. 1974, *Ap. J.*, **192**, 597.
Dickinson, D. F., Gottlieb, C. A., Gottlieb, E. W., and Litvak, M. M. 1976, *Ap. J.*, **206**, 79.
Gatley, I., Becklin, E. E., Matthews, K., Neugebauer, G., Penston, M. V., and Scoville, N. 1974, *Ap. J.* (*Letters*), **191**, L121.
Giguere, P. T., Snyder, L. E., and Buhl, D. 1973, *Ap. J.* (*Letters*), **182**, L11.
Gilmore, W., Zuckerman, B., Turner, B. E., Morris, M., and Palmer, P. 1977, in preparation.
Glassgold, A. E., and Langer, W. D. 1976, *Ap. J.*, **204**, 403.
Gottlieb, C. A., and Ball, J. A. 1973, *Ap. J.* (*Letters*), **184**, L59.
Gottlieb, C. A., Lada, C. J., Gottlieb, E. W., Lilley, A. E., and Litvak, M. M. 1975, *Ap. J.*, **202**, 655.
Green, S. 1975, *Ap. J.*, **201**, 366.
Green, S., and Thaddeus, P. 1974, *Ap. J.*, **191**, 653.
Green, S., Montgomery, J. A., and Thaddeus, P. 1974, *Ap. J.* (*Letters*), **193**, L89.
Herbst, E., and Klemperer, W. 1973, *Ap. J.*, **185**, 505 (HK).
Herbst, E., Bohme, D. K., Payzant, J. D., and Schiff, H. I. 1975, *Ap. J.*, **201**, 603.
Hollis, J. M., Snyder, L. E., Buhl, D., and Giguere, P. T. 1975, *Ap. J.*, **200**, 584.
Kwan, J., and Scoville, N. Z. 1975, *Ap. J.* (*Letters*), **195**, L85.
Leung, C. M., and Liszt, H. S. 1976, *Ap. J.*, **208**, 732.
Morris, M., Palmer, P., Turner, B. E., and Zuckerman, B. 1974, *Ap. J.*, **191**, 349.
Rickard, L. J, Zuckerman, B., and Palmer, P. 1975, *Ap. J.*, **200**, 6.
Saykally, R. J., Dixon, T. A., Anderson, T. G., Szanto, P. G., and Woods, R. C. 1976, *Ap. J.* (*Letters*), **205**, L101.
Schiff, H. I., Hemsworth, R. S., Payzant, J. B., and Bohme, D. K. 1974, *Ap. J.* (*Letters*), **191**, L49.
Snyder, L. E., and Buhl, D. 1973, *Ap. J.* (*Letters*), **185**, L79.
———. 1977, in preparation.
Snyder, L. E., and Hollis, J. M. 1976, *Ap. J.* (*Letters*), **204**, L139.
Snyder, L. E., Hollis, J. M., Lovas, F. J., and Ulich, B. L. 1976, *Ap. J.*, **209**, 67.
Thaddeus, P., Kutner, M. L., Penzias, A. A., Wilson, R. W., and Jefferts, K. B. 1972, *Ap. J.* (*Letters*), **176**, L73.
Thaddeus, P., and Turner, B. E. 1975, *Ap. J.* (*Letters*), **201**, L25.
Tucker, K. D., and Kutner, M. L. 1977, in preparation.
Turner, B. E. 1974, *Ap. J.* (*Letters*), **193**, L83.
Turner, B. E., and Gammon, R. H. 1975, *Ap. J.*, **198**, 71 (TG).
Ulich, B. L., and Haas, R. W. 1976, *Ap. J. Suppl.*, **30**, 247.
Watson, W. D. 1973, *Ap. J.* (*Letters*), **183**, L17.
———. 1974, *Ap. J.*, **188**, 35.
Woods, R. C., Dixon, T. A., Saykally, R. J., and Szanto, P. G. 1975, *Phys. Rev. Letters*, **35**, 1269.
Zuckerman, B., and Palmer, P. 1974, *Ann. Rev. Astr. Ap.*, **12**, 279.
———. 1975, *Ap. J.* (*Letters*), **199**, L35.

P. THADDEUS: Institute for Space Studies, 2880 Broadway, New York, NY 10025
B. E. TURNER: National Radio Astronomy Observatory, Edgemont Road, Charlottesville, VA 22901